PERFORMANCE OF ANALOG FEEDBACK IN CLOSED-LOOP TRANSMIT DIVERSITY SYSTEMS

by

Eddy Chiu
B.A.Sc. (Electronics Engineering), Simon Fraser University, 2003

THESIS SUBMITTED IN PARTIAL FULFILLMENT OF
THE REQUIREMENTS FOR THE DEGREE OF

MASTER OF APPLIED SCIENCE

In the
School
of
Engineering Science

SIMON FRASER UNIVERSITY

Summer 2006

APPROVAL

Name: **Eddy Chiu**

Degree: **Master of Applied Science**

Title of Thesis: **Performance of Analog Feedback in Closed-Loop Transmit Diversity Systems**

Examining Committee:

Chair: **Dr. Jie Liang**
Assistant Professor of the School of Engineering Science

Dr. Paul Ho
Senior Supervisor
Professor of the School of Engineering Science

Dr. James Cavers
Supervisor
Professor of the School of Engineering Science

Dr. Daniel C. Lee
Internal Examiner
Associate Professor of the School of Engineering Science

Date Defended/Approved: July. 10/06

ABSTRACT

Knowledge of channel state information (CSI) at the transmitter can be used for transmit beamforming. However, providing the transmitter with CSI typically requires feedback from the receiver, and this is complicated by low feedback rates. This thesis is concerned with the efficient transmission of CSI in the uplink, and data in the downlink, of a closed-loop transmit diversity system. Two main ideas are explored. First, we consider the employment of analog CSI feedback whereby downlink gain estimates are fed back periodically to the base station at a rate of only one analog symbol per estimate per data frame. Second, we consider the use of position dependent modulation (PDM) to counter the signal to noise ratio variation across a downlink data frame. Simulation results indicated that analog feedback can achieve better bit error rate (BER) than digital feedback, and PDM can attain higher throughput than fixed modulation at a target BER.

Keywords: wireless communication, transmit diversity, CSI feedback, analog feedback, position dependent modulation

ACKNOWLEDGEMENTS

First, I wish to express my sincere appreciation to my senior supervisor, Dr. Paul Ho, for giving me the opportunity to work under his guidance. I am deeply impressed by his knowledge and leadership, and I shall remember the many things he taught me. Special thanks are due to Dr. James Cavers and Dr. Daniel Lee for examining and reviewing this thesis, and to Dr. Jie Liang for chairing my thesis defense. I would also like to thank all my great teachers throughout my years at SFU. Finally, I would like to express my gratitude to my family for their care, encouragement, support, and lucky money (red envelops).

TABLE OF CONTENTS

LIST OF FIGURES

LIST OF TABLES

ABBREVIATIONS

AWGN	Additive white Gaussian noise
BER	Bit error rate
CSI	Channel state information
DD	Differential detection
FDD	Frequency division duplex
I	In-phase
MISO	Multiple-input single-output
MRC	Maximal ratio combining
MMSE	Minimum mean square error
MSDD	Multiple symbol differential detection
MSE	Mean square error
SNR	Signal-to-noise ratio
SISO	Single-input single-output
SIMO	Single-input multiple-output
SQRC	Square root raised cosine
TDD	Time division duplex
Q	Quadrature
iid	Independent and identically distributed
pdf	Probability density function
sps	Symbols per second

NOTATIONS

$E[\cdot]$	Expectation operator
$E[x\|y]$	Expected value of x given the event y
$J_0(\cdot)$	Zero-th order Bessel function of the first kind
$\mathrm{Re}\{\cdot\}$	Real part of a complex number
$\mathrm{Im}\{\cdot\}$	Imaginary part of a complex number
$\Pr\{\cdot\}$	Probability of an event
$diag(a_1, a_2, \ldots, a_N)$	Diagonal matrix containing $a_1, a_2, \ldots, a_N$
$(\cdot)^H$	Hermitian transpose
$(\cdot)^T$	Matrix transpose

CHAPTER 1 INTRODUCTION

In wireless communication systems, the transmitted signal experiences random fluctuations in phase and amplitude – or fading – through the propagation channel. Fading distorts the data embedded in the signal, and causes the signal to lose power and become more vulnerable to noise and interference. At the receiver, the effects of fading need to be accounted for when retrieving data from the received signal. But if the signal power is severely weakened by fading, then the received data is in error with high probability. A practical method for enhancing the reliability and capacity of data transmission is to implement spatial diversity, whereby multiple antennas are deployed at the transmitter and the receiver, and signal processing is applied in conjunction to create one or more better quality communication links.

For personal communication applications, the base station can deploy multiple antennas, whereas mobile units can only use a single antenna due to size and complexity limitations. In the uplink, the mobile unit transmits and the base station receives, and receive diversity can be achieved by efficient combining of the multiple received signals. Conversely, in the downlink, the base station transmits and the mobile unit receives, such that the transmitted signals are received as one combined signal, and pre-transmission processing is required to exploit transmit diversity. In general [1], [2], transmit diversity can be achieved by transmitting orthogonal – and thus separable – signals like space-time coding [3], [4], or by beamforming so that the transmitted signals combine more strongly at the receiver. The latter technique of transmit beamforming requires the base station to

have channel state information (CSI), but offers simple signal processing for data reception, and optimal performance provided that the CSI is sufficiently accurate. In a time division duplex (TDD) system, uplink and downlink transmission share the same frequency band, and so the channels are reciprocal. Therefore, to apply beamforming in downlink transmission, knowledge of the downlink channel can be obtained from the uplink. On the contrary, in a frequency division duplex (FDD) system, uplink and downlink transmission use separated frequency bands, and so the channels are unrelated. Therefore, to apply beamforming in downlink transmission, downlink CSI is estimated at the mobile unit, and transferred to the base station via a feedback link; this results in a closed-loop system.

This thesis is concerned with the efficient transmission of CSI in the uplink, and data in the downlink, of FDD closed-loop transmit diversity systems. We investigate the concept of analog CSI feedback, and demonstrate with computer simulation the resulting downlink performance in terms of error rates and throughput.

1.1 Closed-Loop Transmit Diversity Systems

Previous work on closed-loop transmit diversity systems can be loosely classified into analyses of performance with imperfect CSI, and proposals on improvement of CSI accuracy. The impact of imperfect CSI on error performance is analyzed, for example, in [5]-[7]. Although the error performance analysis carried out in [8] is concerned with open-loop transmit diversity systems, it is also applicable to closed-loop systems. The mutual information of closed-loop systems is investigated in [1], [2], wherein guidelines are given on the accuracy of CSI necessary for transmit beamforming to be favorable. The lack of accuracy of CSI is mainly attributable to low feedback rates, resulting in long

feedback delays. To compensate for feedback delays, as well as to facilitate combined adaptive modulation and transmit diversity, channel prediction can be used as studied in [7], [9]. Furthermore, in traditional closed-loop systems, CSI is fed back in digital representation; limited by low feedback rates, CSI needs to be digitized with low precision, resulting in significant quantization error. To minimize quantization error, CSI can be efficiently quantized using heuristic search (see e.g., [6], [11]) or suitably designed codebooks (see e.g., [2], [10], [12] and [13]).

Recently, the concept of analog CSI feedback under a multi-user operating environment is explored in [14]. It is suggested that analog feedback enables CSI to be made available to the base station in more timely and accurate fashion than digital feedback. But regardless of the nature of the feedback scheme, the feedback rate is typically much lower than the baud rate, and as a result the accuracy of CSI varies significantly over a feedback period. As pointed out in [10], this important – yet often neglected – issue of periodic variation in CSI accuracy should be taken into account when analyzing and designing closed-loop systems.

1.2 Thesis Outline

This thesis is organized as follows. Chapter 2 covers the background material and establishes the models and conventions that will be used throughout this thesis. Chapter 3 introduces the proposed closed-loop transmit diversity system based on an analog CSI feedback scheme, which requires a low feedback rate and avoids unrecoverable distortion as in traditional digital feedback. Performance results of the proposed system are presented and compared against those obtained using digital feedback under the same operating conditions. Chapter 4 identifies and provides solutions for various issues

associated with the proposed system, most importantly of which are the periodic variation in CSI accuracy and the large dynamic range of analog feedback symbols. Finally, Chapter 5 summarizes the work in the thesis and provides suggestion for future work.

1.3 Contributions of this Thesis

We investigated two main topics: i) the concept of analog feedback and ii) the mitigation of the impact of periodic variation in CSI accuracy. As indicated in Section 1.1, these issues – so strangely – have hardly been studied. We only recently became aware of [14], which explores the mean square error (MSE) of CSI using analog feedback, provided that the mobile transmitters can accommodate the dynamic range requirements. This thesis complements the findings in [14] in the way that we consider the bit error rate (BER) and throughput of closed-loop systems that use analog feedback, make comparisons to systems that use digital feedback, and examine the impact of limiting the dynamic range of the analog feedback symbols. On the other hand, the issue of periodic variation in CSI accuracy is raised in [10] but a solution is not provided. Based on the notion that it is inefficient to use the same modulation over a feedback period, we propose to use a variable rate position dependent modulation scheme and thereby improve the achievable throughput.

CHAPTER 2 BACKGROUND

In this chapter, we cover the background material and establish the models and conventions that will be used throughout this thesis. The topics are organized as follows. The baseband representation of bandpass systems is reviewed in Section 2.1. Downlink transmission is covered in two sections, the basic single-input single-output (SISO) model is discussed in Section 2.2, and the generalized multiple-input single-output (MISO) model is discussed in Section 2.3. Uplink transmission is based on a single-input multiple-output (SIMO) model and is presented in Section 2.4. Channel estimation is considered in Section 2.5. Simulation conventions are defined in Section 2.6, followed by a chapter summary in Section 2.7.

2.1 Baseband Representation of Bandpass Systems

In narrowband digital communication systems, data is sent by modulating a carrier with an information signal, whose bandwidth is much smaller than the carrier frequency. The modulated waveform is called a bandpass signal and is expressed in the form

$$\begin{aligned} \tilde{s}(t) &= A(t)\cos(2\pi f_c t + \phi(t)) \\ &= \mathrm{Re}\{s(t)e^{j2\pi f_c t}\}, \end{aligned} \tag{1}$$

where $A(t)$ and $\phi(t)$ are the amplitude and phase of the information signal, respectively, f_c is the carrier frequency, $s(t) = A(t)e^{j\phi(t)}$ is the complex baseband equivalent of $\tilde{s}(t)$, and $\mathrm{Re}\{\cdot\}$ is the real part of a complex number. For mathematical convenience, it is

more desirable to represent modulated signals and channels by their baseband equivalents. Therefore, we adopt the complex baseband representation for the rest of this thesis, and deal only with transmission of the equivalent low pass signals through the equivalent low pass channels.

2.2 Downlink SISO Transmission Model

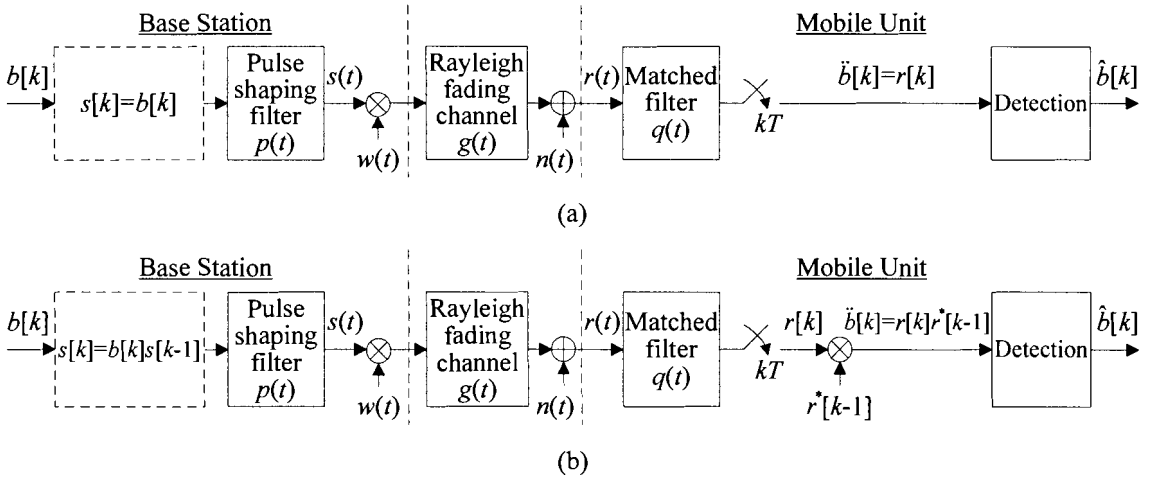

Figure 2-1. Downlink SISO transmission model. (a) Coherent detection of PSK symbols. (b) Differential encoding and differential detection of PSK symbols.

In this thesis, downlink transmission follows the basic model illustrated in Figure 2-1. For simplicity, a SISO link with one transmit antenna and one receive antenna is presented here, and general MISO links with multiple transmit antennas are discussed in the next section. At discrete time k, binary bits are Gray mapped into a MPSK data symbol $b[k]$ from the set $\left\{e^{j2\pi c/M}; c = 0,1,\ldots,M-1\right\}$. The data symbol is either directly transmitted as $s[k] = b[k]$ (see Figure 2-1 (a)), or differentially encoded to form the transmitted symbol $s[k] = b[k]s[k-1]$ (see Figure 2-1 (b)), where $s[k-1]$ is the previous

transmitted symbol. Modulating $s[k]$ by a square root raised cosine (SQRC) pulse shaping filter $p(t)$ with unit energy $\int p^2(t)dt = 1$, the transmitted signal is formed as

$$s(t) = \sum_k s[k]p(t - kT), \tag{2}$$

where $1/T$ is the baud rate.

We assume a frequency-nonselective Rayleigh fading channel [17] with additive white Gaussian noise (AWGN). To take into account the effects of fading, a piecewise constant transmission weighting pattern $w(t)$ is applied to the transmitted signal $s(t)$. This transmission weight is determined from CSI fed back from the mobile unit, and ideally proportional to the conjugate of the channel gain. Its mathematical expression is provided in the next section. It follows that the weighted transmitted signal arrives at the mobile unit as

$$r(t) = w(t)g(t)s(t) + n(t), \tag{3}$$

where $g(t)$ is the channel gain and $n(t)$ is the noise term. The channel gain $g(t)$ is a complex Gaussian random process with zero mean and variance $\sigma_g^2 = \frac{1}{2}E\left[|g(t)|^2\right]$, where $E[\cdot]$ is the expectation operator. It is assumed that $g(t)$ remains constant within each symbol interval T but can vary from interval to interval. Moreover, under the assumption of isotropic scattering and vertical polarized antenna, $g(t)$ has a U-shaped spectrum with bandwidth equal to the Doppler frequency f_d, and an Jakes autocorrelation [17 (1.3-1)]

$$\phi_g(\tau) = \frac{1}{2}E\left[g(t)g^*(t-\tau)\right] = \sigma_g^2 J_0(2\pi f_d \tau), \tag{4}$$

where $J_0(\cdot)$ is the zero-th order Bessel function of the first kind. On the other hand, the noise term $n(t)$ is a complex white Gaussian random process with zero mean and a power spectral density of unity.

At the mobile unit, the received signal $r(t)$ is passed through an SQRC matched filter $q(t) = p(-t)$, whose output is sampled at $t = kT$ to give the received symbol

$$r[k] = w[k]g[k]s[k] + n[k], \tag{5}$$

where $w[k]$ and $g[k]$ are samples of $w(t)$ and $g(t)$, respectively, and $n[k]$ is a filtered noise sample. It can be shown that the channel gain sample $g[k]$ has an autocorrelation function of

$$\phi_g[d] = \frac{1}{2}E\left[g[k]g^*[k-d]\right] = \sigma_g^2 J_0(2\pi f_d dT), \tag{6}$$

and the noise sample $n[k]$ has variance of $\sigma_n^2 = 1$. If the data symbol is directly transmitted, then coherent detection is employed (see Figure 2-1 (a)); the received symbol is directly used as the decision variable $\ddot{b}[k] = r[k]$ for detecting the data symbol estimate $\hat{b}[k]$. On the contrary, if the data symbol is differentially encoded, then conventional 2-symbol differential detection (DD) is employed (see Figure 2-1 (b)); the received symbol $r[k]$ is multiplied by the conjugate of the previous received symbol $r^*[k-1]$ to form the decision variable $\ddot{b}[k] = r[k]r^*[k-1]$ for detecting the data symbol estimate $\hat{b}[k]$. Differential encoding and detection are intended to compensate for the residual phase shift on the transmitted symbol $s[k]$, when the transmission weight $w[k]$ cannot cancel out the phase shift caused by the channel gain $g[k]$.

2.3 Downlink MISO Transmission Model

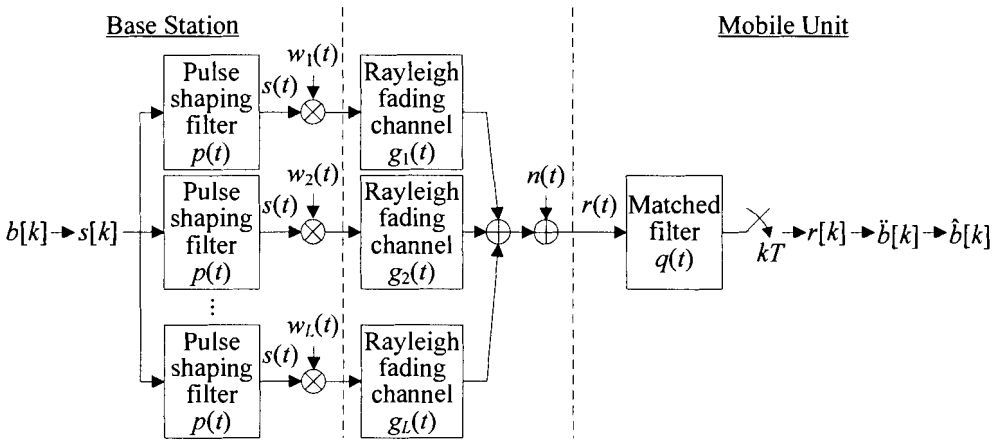

Figure 2-2. Downlink MISO transmission model.

The primary objective of this thesis is downlink data transmission, from the base station via multiple antennas, to a mobile unit equipped with one receive antenna. Therefore, we assume the base station is equipped with L antennas for the rest of this thesis. The MISO link realized is depicted in Figure 2-2, where the transmitted signal is sent over L channels with the same fading characteristics as the SISO link presented in the last section, and the noise term $n(t)$ is added to the composite signal that arrives at the mobile unit. Assuming that the base station antennas are sufficiently separated in space, the channel gains $g_l(t)$, $l = 1,2,\ldots,L$, are independent and identically distributed (iid). The set of transmission weights $w_l(t)$, $l = 1,2,\ldots,L$, are applied to the transmitted signals such that they can be combined with a beamforming effect. Consequently, at discrete time k, the mobile unit receives the symbol

$$r[k] = G[k]s[k] + n[k], \tag{7}$$

where

$$G[k] = \sum_{l=1}^{L} w_l[k] g_l[k] \tag{8}$$

is the beamformed gain, and the $g_l[k]$'s and the $w_l[k]$'s are the channel gains and transmission weights at $t = kT$, respectively. We impose the constraint $\sum_{l=1}^{L} |w_l[k]|^2 = 1$ to maintain a constant total power of

$$\begin{aligned} \sigma_G^2 &= \frac{1}{2} E\left[|G[k]|^2\right] = \frac{1}{2} E\left[\left|\sum_{l=1}^{L} w_l[k] g_l[k]\right|^2\right] \\ &= \sum_{l=1}^{L}\sum_{p=1}^{L} w_l[k] w_p^*[k] \frac{1}{2} E\left[g_l[k] g_p^*[k]\right] \\ &= \sum_{l=1}^{L}\sum_{p=1}^{L} w_l[k] w_p^*[k] \sigma_g^2 \delta(l-p) = \sigma_g^2 \sum_{l=1}^{L} |w_l[k]|^2 \\ &= \sigma_g^2 \end{aligned} \tag{9}$$

in the MISO link that is independent of the number of base station antennas L. This implies the average power per base station antenna is σ_g^2 / L. The effectiveness of beamforming, intuitively, depends on how well the transmission weights match the channel conditions, which we quantify below.

In the ideal case that the base station has perfect CSI, it can determine the transmission weights that enable the diversity branches to combine into an effective line-of-sight beamformed gain with the largest possible power. Bearing this objective, optimal transmission weights should be proportional to the conjugate of the channel gains; specifically,

$$w_l[k] = \frac{g_l^*[k]}{\sqrt{\sum_{a=1}^{L} |g_a[k]|^2}}, \; l = 1,2,\ldots,L, \tag{10}$$

and the resultant beamformed gain is

$$G[k]=\sum_{l=1}^{L}\frac{g_l^*[k]}{\sqrt{\sum_{a=1}^{L}|g_a[k]|^2}}g_l[k]=\frac{\sum_{l=1}^{L}|g_l[k]|^2}{\sqrt{\sum_{a=1}^{L}|g_a[k]|^2}} \tag{11}$$
$$=\sqrt{\sum_{l=1}^{L}|g_l[k]|^2}.$$

Since $G[k]$ is real and does not cause any phase shift on the transmitted symbol $s[k]$, the received symbol can be readily used as the decision variable for coherent detection

$$\ddot{b}[k]=r[k]=G[k]s[k]+n[k]$$
$$=s[k]\sqrt{\sum_{l=1}^{L}|g_l[k]|^2}+n[k].$$

Thus, the instantaneous SNR of the decision variable, conditioned on the channel gains $g_l[k]$'s, is

$$\gamma[k]=\frac{\frac{1}{2}\left|s[k]\sqrt{\sum_{l=1}^{L}|g_l[k]|^2}\right|^2}{\frac{1}{2}E\left[|n[k]|^2\right]}=\frac{\frac{1}{2}\sum_{l=1}^{L}|g_l[k]|^2}{\sigma_n^2} \tag{12}$$
$$=\frac{1}{2}\sum_{l=1}^{L}|g_l[k]|^2,$$

which equals to the sum of the powers of the diversity branches

On the other hand, in the realistic case that the base station has imperfect CSI, we model each channel gain $g_l[k]$ as the sum of its estimate $\hat{g}_l[k]$ and an uncorrelated estimation error $e_l[k]$, i.e.,

$$g_l[k] = \hat{g}_l[k] + e_l[k],\ l = 1,2,\ldots,L. \tag{13}$$

The channel gain estimates $\hat{g}_l[k]$'s and the estimation errors $e_l[k]$'s are complex Gaussian random variables with zero mean and variances

$$\sigma^2_{\hat{g}[k]} = \frac{1}{2}E\left[|\hat{g}_l[k]|^2\right] = \rho^2_{g\hat{g}}[k]\sigma^2_g \tag{14}$$

and

$$\sigma^2_{e[k]} = \frac{1}{2}E\left[|e_l[k]|^2\right] = \left(1 - \rho^2_{g\hat{g}}[k]\right)\sigma^2_g, \tag{15}$$

respectively, where $\rho_{g\hat{g}}[k]$ is the correlation coefficient between the true channel gain $g_l[k]$ and its estimate $\hat{g}_l[k]$. Note that $\rho_{g\hat{g}}[k]$ is a function of discrete time k, and so the variances in (14) and (15) are not constant. For example, channel gain estimates obtained via linear prediction exhibit this behavior, as we shall elaborate in Section 3.1. But similar to the true channel gains, the $\hat{g}_l[k]$'s and $e_l[k]$'s are iid.

The beamformed gain with channel gains expressed in terms of estimates and estimation errors is

$$\begin{aligned} G[k] &= \sum_{l=1}^{L} w_l[k]\left(\hat{g}_l[k] + e_l[k]\right) \\ &= \sum_{l=1}^{L} w_l[k]\hat{g}_l[k] + \sum_{l=1}^{L} w_l[k]e_l[k]. \end{aligned}$$

The transmission weights, to the best of the base station's knowledge, based on the channel gain estimates $\hat{g}_l[k]$'s are

$$w_l[k] = \frac{\hat{g}_l^*[k]}{\sqrt{\sum_{a=1}^{L} |\hat{g}_a[k]|^2}}, \; l = 1,2,\ldots,L. \tag{16}$$

Consequently,

$$\begin{aligned} G[k] &= \sum_{l=1}^{L} \frac{\hat{g}_l^*[k]}{\sqrt{\sum_{a=1}^{L} |\hat{g}_a[k]|^2}} \hat{g}_l[k] + \sum_{l=1}^{L} \frac{\hat{g}_l^*[k]}{\sqrt{\sum_{a=1}^{L} |\hat{g}_a[k]|^2}} e_l[k] \\ &= \sqrt{\sum_{l=1}^{L} |\hat{g}_l[k]|^2} + U[k]. \end{aligned} \tag{17}$$

Let the first and second terms in (17) be referred to as the direct and diffuse components of the beamformed gain, respectively. The diffuse component $U[k]$ is the weighted sum of the estimation errors $e_l[k]$'s and is therefore a complex random process with zero mean. When conditioned on the channel gain estimates $\hat{g}_l[k]$'s, $U[k]$ is complex Gaussian distributed with variance

$$\begin{aligned} \sigma_{U[k]}^2 &= \frac{1}{2} E\left[|U[k]|^2\right] = \frac{1}{2} E\left[\left| \sum_{l=1}^{L} \frac{\hat{g}_l^*[k]}{\sqrt{\sum_{a=1}^{L} |\hat{g}_a[k]|^2}} e_l[k] \right|^2\right] \\ &= \sum_{l=1}^{L} \sum_{p=1}^{L} \frac{\hat{g}_l^*[k] \hat{g}_p[k]}{\sum_{a=1}^{L} |\hat{g}_a[k]|^2} \frac{1}{2} E\left[e_l[k] e_p^*[k]\right] \\ &= \sum_{l=1}^{L} \sum_{p=1}^{L} \frac{\hat{g}_l^*[k] \hat{g}_p[k]}{\sum_{a=1}^{L} |\hat{g}_a[k]|^2} \sigma_{e[k]}^2 \delta(l-p) = \frac{\sum_{l=1}^{L} |\hat{g}_l[k]|^2}{\sum_{a=1}^{L} |\hat{g}_a[k]|^2} \sigma_{e[k]}^2 \\ &= \sigma_{e[k]}^2 \end{aligned} \tag{18}$$

that is equal to the variance of the $e_l[k]$'s. Furthermore, since $U[k]$ is complex, it causes a phase shift on the transmitted symbol $s[k]$.

If we employ coherent detection based directly on the received symbol, then the decision variable is

$$\begin{aligned}\ddot{b}[k] = r[k] &= G[k]s[k] + n[k] \\ &= s[k]\sqrt{\sum_{l=1}^{L}|\hat{g}_l[k]|^2} + s[k]U[k] + n[k] \\ &\equiv s[k]\sqrt{\sum_{l=1}^{L}|\hat{g}_l[k]|^2} + U[k] + n[k],\end{aligned}$$

where $s[k]$ is absorbed into $U[k]$ on the third step. The instantaneous SNR, conditioned on the channel gain estimates $\hat{g}_l[k]$'s, is degraded from (12) to

$$\begin{aligned}\gamma[k] &= \frac{\frac{1}{2}\left|s[k]\sqrt{\sum_{l=1}^{L}|\hat{g}_l[k]|^2}\right|^2}{\frac{1}{2}E\left[|U[k]+n[k]|^2\right]} = \frac{\frac{1}{2}\sum_{l=1}^{L}|\hat{g}_l[k]|^2}{\sigma_{e[k]}^2+\sigma_n^2} \\ &= \frac{1}{2\left(\sigma_{e[k]}^2+1\right)}\sum_{l=1}^{L}|\hat{g}_l[k]|^2.\end{aligned} \tag{19}$$

As (19) reveals, channel estimation error simultaneously reduces the signal power and increases interference.

If we employ conventional DD on differentially encoded PSK symbols, then the decision variable is

$$\begin{aligned}\ddot{b}[k] = r[k]r^*[k-1] &= \left(G[k]s[k]+n[k]\right)\left(G^*[k-1]s^*[k-1]+n^*[k-1]\right) \\ &= G[k]G^*[k-1]s[k]s^*[k-1] + G[k]s[k]n^*[k-1] \\ &\quad + G^*[k-1]s^*[k-1]n[k] + n[k]n^*[k-1].\end{aligned}$$

Under slow fading, $G[k-1] \approx G[k]$, absorbing $s[k]$ into $n^*[k-1]$ and $s^*[k-1]$ into $n[k]$, and making the approximation to neglect the product noise term, the decision variable becomes

$$\ddot{b}[k] \approx |G[k]|^2 b[k] + G^*[k]n[k] + G[k]n^*[k-1].$$

The instantaneous SNR conditioned on the beamformed gain $G[k]$ is

$$\gamma[k] = \frac{\frac{1}{2}\left||G[k]|^2 b[k]\right|^2}{\frac{1}{2}E\left[\left|G^*[k]n[k] + G[k]n^*[k-1]\right|^2\right]} = \frac{\frac{1}{2}|G[k]|^2}{2\sigma_n^2}$$
$$= \frac{1}{4}\left|\sqrt{\sum_{l=1}^{L}|\hat{g}_l[k]|^2} + U[k]\right|^2.$$

Furthermore, averaging out the effect of the diffuse component $U[k]$, the instantaneous SNR conditioned on the $\hat{g}_l[k]$'s becomes

$$\gamma[k] = \frac{1}{4}E\left[\left|\sqrt{\sum_{l=1}^{L}|\hat{g}_l[k]|^2} + U[k]\right|^2\right]$$
$$= \frac{1}{4}\sum_{l=1}^{L}|\hat{g}_l[k]|^2 + \frac{1}{4}E\left[|U[k]|^2\right] \qquad (20)$$
$$= \frac{1}{4}\sum_{l=1}^{L}|\hat{g}_l[k]|^2 + \frac{1}{2}\sigma_{e[k]}^2.$$

Comparing (19) and (20), unless channel estimation is highly accurate and $\sigma_{e[k]}^2$ is relatively small, it is much more promising to employ conventional DD than coherent detection based directly on the received symbol. Note that under fast fading, whereby channel gains can change substantially between consecutive symbol intervals, the decorrelation between $G[k-1]$ and $G[k]$ has to be taken into account.

2.4 Uplink Transmission Model

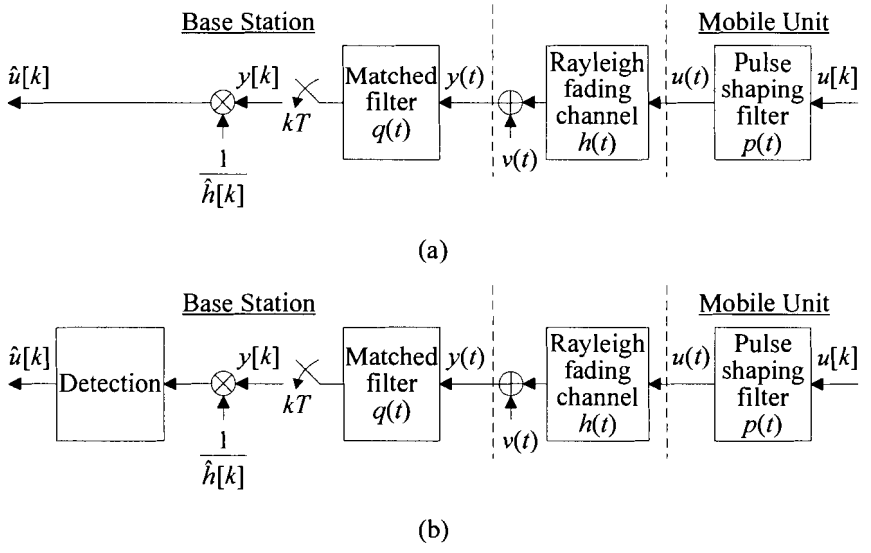

Figure 2-3. Uplink SISO transmission model. (a) Analog CSI feedback. (b) Digital CSI feedback.

To facilitate beamforming in downlink transmission, downlink CSI is estimated at the mobile unit and fed back to the base station in the uplink. For simplicity, consider first the uplink SISO transmission model illustrated in Figure 2-3. The CSI symbol $u[k]$, transmitted at discrete time k, is either in analog form or in digital form. The mean magnitude square of $u[k]$ is normalized to unity, i.e., $E\left[|u[k]|^2\right]=1$. Furthermore, in digital form, $u[k]$ can be a KPSK symbol from the set $\left\{e^{j2\pi c/K}; c=0,1,\ldots,K-1\right\}$, or a square KQAM symbol with in-phase (I) and quadrature (Q) components from the set $\left\{\pm c,\pm 3c,\ldots,\pm\left(\sqrt{K}-1\right)c; c=\sqrt{3/2(K-1)}\right\}$. After pulse-shaping, the transmitted signal $u(t)$ is sent over a frequency-nonselective Rayleigh fading channel with AWGN. It follows that $u(t)$ arrives at the base station as

$$y(t)=h(t)u(t)+v(t), \tag{21}$$

where $h(t)$ is the uplink channel gain and $v(t)$ is the noise term. The channel gain $h(t)$ is a complex Gaussian random process with zero mean, variance $\sigma_h^2 = \frac{1}{2}E\left[|h(t)|^2\right]$, and a Jakes autocorrelation

$$\phi_h(\tau) = \frac{1}{2}E\left[h(t)h^*(t-\tau)\right] = \sigma_h^2 J_0(2\pi f_d \tau). \tag{22}$$

On the other hand, the noise term $v(t)$ is a zero mean complex white Gaussian random process with a power spectral density of unity.

At the base station, after matched filtering the received signal $y(t)$ and sampling the filter output at $t = kT$, the received symbol is obtained as

$$y[k] = h[k]u[k] + v[k], \tag{23}$$

where the channel gain sample $h[k]$ has an autocorrelation function of

$$\phi_h[d] = \frac{1}{2}E\left[h[k]h^*[k-d]\right] = \sigma_h^2 J_0(2\pi f_d dT), \tag{24}$$

and the noise sample $v[k]$ has variance of $\sigma_v^2 = 1$. Based on the channel gain estimate $\hat{h}[k]$, the effects of fading are accounted for by normalizing the received symbol as $y[k]/\hat{h}[k]$. If the CSI symbol is in analog form (see Figure 2-3 (a)), then $y[k]/\hat{h}[k]$ is used directly as the CSI symbol estimate $\hat{u}[k]$. On the contrary, if the CSI symbol is in digital form (see Figure 2-3 (b)), then $y[k]/\hat{h}[k]$ is used as the decision variable for detecting the CSI symbol estimate $\hat{u}[k]$.

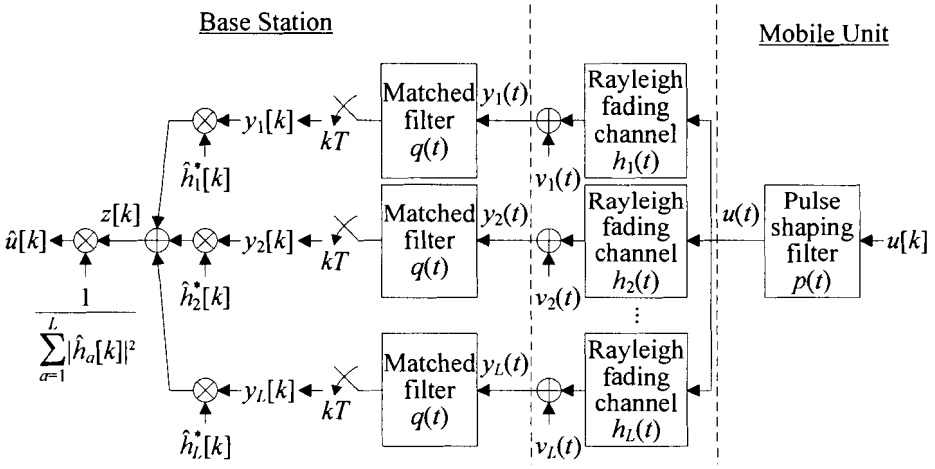

Figure 2-4. Uplink SIMO transmission model.

The general uplink SIMO transmission model is illustrated in Figure 2-4, where the transmitted signal is received from L channels with the same fading characteristics as the SISO link, and the received signals are corrupted by additive noise. In addition, the channel gains $h_q(t)$, $q = 1,2,\ldots,L$, as well as the noise terms $v_q(t)$, $q = 1,2,\ldots,L$, are iid. Consequently, at discrete time k, the base station receives the set of symbols

$$y_q[k] = h_q[k]u[k] + v_q[k],\ q = 1,2,\ldots L, \tag{25}$$

where the $h_q[k]$'s and the $v_q[k]$'s are the channel gains and noise terms at $t = kT$, respectively. Maximal ratio combining (MRC) of the received symbols is performed using the channel gain estimates $\hat{h}_q[k]$'s, i.e.,

$$\begin{aligned} z[k] &= \sum_{q=1}^{L} \hat{h}_q^*[k] y_q[k] \\ &= \sum_{q=1}^{L} \hat{h}_q^*[k]\left(h_q[k]u[k] + v_q[k]\right), \end{aligned} \tag{26}$$

and amplitude fading is accounted for by normalizing $z[k]$ to

$$z[k] \Big/ \sum_{a=1}^{L} \left|\hat{h}_a[k]\right|^2 . \tag{27}$$

This normalized symbol is then used directly as the CSI symbol estimate $\hat{u}[k]$ if the CSI symbol is in analog form, or used as the decision variable for detecting $\hat{u}[k]$ if the CSI symbol is in digital form.

2.5 Channel Estimation

From the description of the transmission models, both the base station and the mobile unit need to perform channel estimation. A simple pilot assisted scheme is used [7], [18], whereby pilot symbols are inserted into the transmitted symbol stream at a rate higher than the Nyquist rate of the channel gain process to facilitate periodic estimation of downlink/uplink gains. As we shall elaborate in Section 3.1, linear prediction filters can be used on the pilot estimates to obtain optimal gain estimates at the data symbols.

In the downlink, since the transmitted symbols from different antennas are received as one composite symbol, multi-symbol and orthogonal pilot sequences are required to achieve the separability at the receiver for estimating the individual channels. Suppose that the L-symbol long pilot sequences $\mathbf{p}_1 = [1\,0\,0\ldots0]$, $\mathbf{p}_2 = [0\,1\,0\ldots0\,0]$, ..., $\mathbf{p}_L = [0\,0\ldots0\,1]$ are transmitted between frames of T_{Fr} seconds, or N symbol intervals, as shown in Figure 2-5 (a). Since the channel gains have a U-shaped spectrum with bandwidth equal to the Doppler frequency f_d, the Nyquist sampling criterion requires a pilot frame rate of $1/T_{Fr} \geq 2f_d$. In the m^{th} frame, let the downlink gains affecting the pilot sequences transmitted from different antennas be represented by the diagonal matrix $\mathbf{G}_l[m] = diag(g_l[mN], g_l[mN+1], \ldots, g_l[mN+(L-1)])$, $l = 1,2,\ldots,L$, the white noise

terms be denoted by $\mathbf{n}[m] = [n[mN]\, n[mN+1] \ldots n[mN+(L-1)]]$, so the pilot symbols are received by the mobile unit as $\mathbf{r}[m] = \sum_{l=1}^{L} \mathbf{p}_l \mathbf{G}_l[m] + \mathbf{n}[m]$. Consequently, downlink gain estimates can be acquired as

$$\ddot{g}_l[mN+(l-1)] = g_l[mN+(l-1)] + n[mN+(l-1)],\ l = 1,2,\ldots,L, \tag{28}$$

which have zero mean and variance $\sigma_{\ddot{g}}^2 = \sigma_g^2 + \sigma_n^2$.

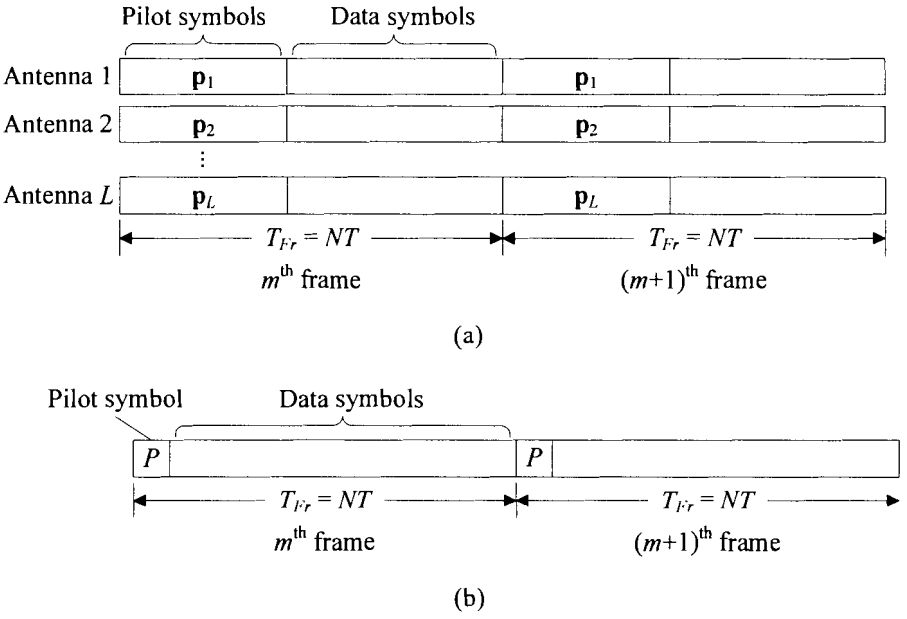

Figure 2-5. Data frame structure (a) in the downlink and (b) in the uplink.

In the uplink, it is sufficient to transmit one pilot symbol per T_{Fr} seconds frame of N symbols, provided that the Nyquist sampling criterion is satisfied as shown in Figure 2-5 (b). The unit energy pilot symbol P is received by the base station in the m^{th} frame as $y_q[mN] = h_q[mN]P + v_q[mN]$ from each channel. Consequently, uplink gain estimates can be acquired as

$$\hat{h}_q[mN] = h_q[mN] + v_q[mN],\ q = 1,2,\ldots,L, \tag{29}$$

which have zero mean and variance $\sigma_{\hat{h}}^2 = \sigma_h^2 + \sigma_v^2$. As a final remark we reiterate that, by nature of FDD, knowledge obtained for uplink gains cannot be applied to infer the downlink gains, and vice versa.

2.6 Simulation Conventions

Throughout this thesis, performance results are obtained by computer simulations with the following conventions. Downlink error rates are presented in terms of the average BER over the downlink frame. On the other hand, downlink throughput is presented in terms of the average number of data bits per symbol interval of T seconds, such that the capacity lost in transmitting the pilot sequences is taken into account. Results are reported versus the downlink symbol SNR defined as

$$\left(\frac{\text{Frame size}}{\text{Data symbols per downlink frame}}\right)\frac{\sigma_g^2}{\sigma_n^2},$$

such that the energy consumed in transmitting the pilot sequences is taken into account. As per (9) the average transmit power per downlink transmitter is σ_g^2/L, and similarly we set the transmit power of the uplink transmitter to $\sigma_h^2 = \sigma_g^2/L$; therefore, uplink SNR is linearly proportional to downlink SNR.

2.7 Summary

The main theme of this chapter is to establish the signal and system models studied in this thesis. The downlink is modelled as a MISO link that exploits transmit beamforming by applying a set of transmission weights on the signals transmitted via the

different antennas, and thereby reinforce the composite signal arriving at the receiver. The transmission weights are determined from downlink CSI estimated by the mobile unit and fed back over the uplink either in analog form or in digital form. The uplink is modelled as a SIMO link that exploits receive diversity by applying MRC of the multiple received signals. To facilitate acquiring downlink and uplink CSI, we make use of standard pilot assisted channel estimation techniques. In this chapter, downlink and uplink transmissions are discussed separately; in the next chapter, we shall explain in detail the closed-loop operation integrating the downlink and the uplink.

CHAPTER 3 PROPOSED CLOSED-LOOP TRANSMIT DIVERSITY SYSTEM

In order to capitalize on the potential of beamforming in downlink data transmission, it is required that the base station has accurate feedback CSI. However, high precision digital feedback imposes significant overhead on uplink throughput. Moreover, if channel conditions change considerably within a short time, then the feedback CSI quickly becomes outdated. To cope with these limitations, we propose a closed-loop transmit diversity system that uses an analog CSI feedback scheme, and incorporates channel prediction. We shall demonstrate that this analog feedback scheme usually requires fewer feedback symbols than digital feedback at a given distortion level, or it causes lower distortion on the feedback CSI than digital feedback when both are implemented with the same number of feedback symbols. On the other hand, channel prediction enables the calculation of adaptive transmission weights, and thus the sustainment of the effectiveness of beamforming between periodic feedback CSI updates.

This chapter is organized as follows. The proposed analog feedback closed-looped system is introduced in Section 3.1. For reference, the digital feedback counterpart of the proposed system is presented in Section 3.2. Computer simulation results and discussions are provided in Section 3.3, followed by a chapter summary in Section 3.4.

3.1 Analog CSI Feedback

The loss of fidelity in feedback digital CSI can be attributed to inefficient mapping of CSI into feedback symbols, feedback errors, and delay. By digital feedback, CSI is quantized and then modulated into QAM or PSK feedback symbols. To lessen the impact of quantization error, the CSI can be encoded with more bits. Then to improve resilience to feedback error, the codeword can be channel coded, and the feedback symbols can be modulated using a smaller constellation. But the number of feedback symbols and feedback delay increase accordingly, thus impose greater overhead on uplink throughput and reduce the timeliness of the feedback CSI.

How can we simultaneously reduce distortion on the feedback CSI and use a smaller number of feedback symbols? To do so, we consider the concept of analog feedback, whereby each downlink complex gain estimate is fed back to the base station as is, except for amplitude scaling. This approach requires only one feedback symbol per base station antenna per data frame. In addition, unlike digital feedback, analog feedback offers excellent asymptotic performance as there is no unrecoverable quantization error. A drawback of analog feedback though is that the feedback symbols have high instantaneous power, but a simple resolution to this problem is presented in Section 4.4.

The proposed closed-loop system is modelled in Figure 3-1 that shows details of the downlink, and the timing between downlink channel estimation and CSI feedback is outlined in Figure 3-2. As indicated in Section 2.5, the mobile unit uses the L-symbol long orthogonal pilot sequences that are inserted into the downlink symbol stream at a rate of $1/T_{Fr}$ to periodically estimate the downlink gains $g_l[k]$, $l = 1,2,\ldots,L$, where the frame rate $1/T_{Fr}$ is higher than the Nyquist rate, and the frame duration of T_{Fr} seconds is

equal to N symbol intervals. It follows from (28) that the downlink gain estimates in the m^{th} frame are acquired by the mobile unit as

$$\ddot{g}_l[mN+(l-1)] = g_l[mN+(l-1)] + n[mN+(l-1)],\ l=1,2,\ldots,L,$$

which have zero mean and variance $\sigma_{\ddot{g}}^2 = \sigma_g^2 + \sigma_n^2$. The mobile unit processes the $\ddot{g}_l[mN+(l-1)]$'s into L CSI symbols $u_1, u_2, \ldots, u_L$, and feeds them back to the base station at the start of the next uplink frame. The CSI symbols are generated by amplitude scaling the downlink gain estimates to have unit average energy as defined in the transmission model in Section 2.4. We assume the mobile unit acquires the downlink gain estimates after it receives all L pilot symbols, and all the feedback symbols arrive at the base station after a delay of T_{Fb} seconds equal to D symbol intervals. This feedback delay comprises of both processing and transmission time so $D \geq L$. Incorporating the delay, the analog CSI symbols u_l's can now be expressed as uplink symbols as

$$u[mN+(l-1)+D] = \frac{\ddot{g}_l[mN+(l-1)]}{\sqrt{2\sigma_{\ddot{g}}^2}},\ l=1,2,\ldots,L, \tag{30}$$

whose average energy is

$$\begin{aligned}
&\frac{1}{L}\sum_{l=1}^{L} E\left[|u[mN+(l-1)+D]|^2\right] \\
&= \frac{1}{L}\sum_{l=1}^{L} E\left[\left|\frac{\ddot{g}_l[mN+(l-1)]}{\sqrt{2\sigma_{\ddot{g}}^2}}\right|^2\right] \\
&= \frac{1}{L}\sum_{l=1}^{L} \frac{1}{\sigma_{\ddot{g}}^2}\frac{1}{2} E\left[|\ddot{g}_l[mN+(l-1)]|^2\right] = \frac{1}{L}\sum_{l=1}^{L}\frac{\sigma_{\ddot{g}}^2}{\sigma_{\ddot{g}}^2} \\
&= 1.
\end{aligned}$$

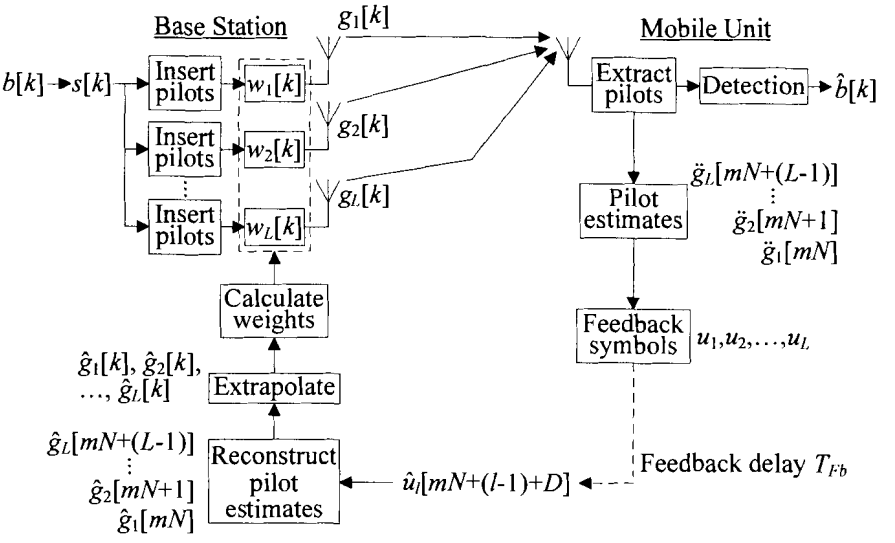

Figure 3-1. Proposed closed-loop system using analog feedback.

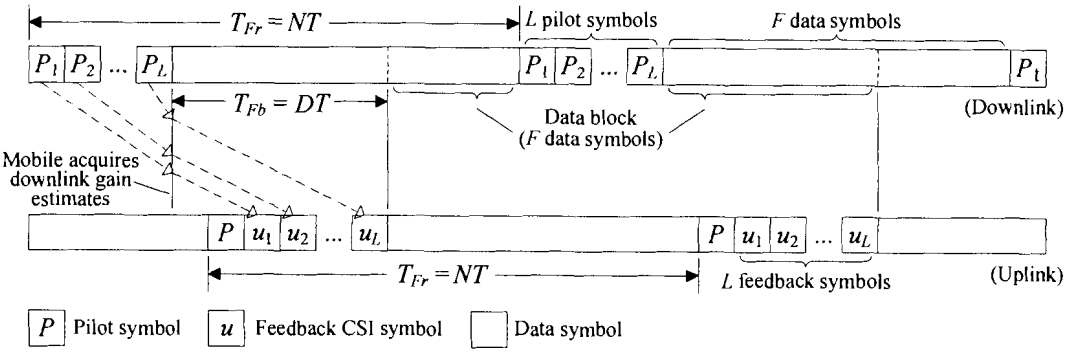

Figure 3-2. Closed-loop data frame structure using analog feedback.

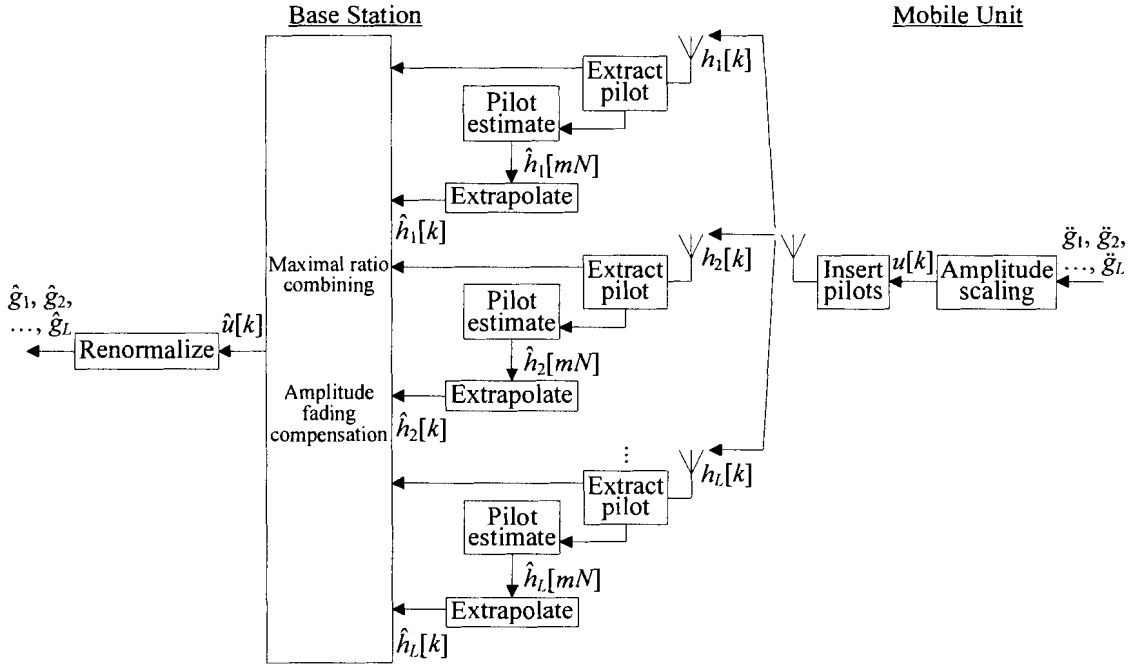

Figure 3-3. Uplink model of the proposed closed-loop system using analog feedback.

Transmission of the CSI symbol $u[k]$ in the uplink is modelled in Figure 3-3. Again as indicated in Section 2.5, the base station uses the pilot symbols that are inserted into the uplink symbol stream once every T_{Fr} seconds, or N symbols, to periodically estimate the uplink gains $h_q[k]$, $q = 1,2,\ldots,L$. It follows from (29) that the uplink gain estimates in the m^{th} frame are acquired by the base station as

$$\hat{h}_q[mN] = h_q[mN] + v_q[mN],\ q = 1,2,\ldots,L,$$

which have zero mean and variance $\sigma_{\hat{h}}^2 = \sigma_h^2 + \sigma_v^2$. Linear prediction is used to extrapolate from the periodic uplink gain estimates $\hat{h}_q[mN]$'s the gain estimates $\hat{h}_q[k]$'s at the data symbol positions, which in turn are used to perform MRC of the received symbols and to compensate for amplitude fading. So from (26) and (27), the CSI symbol estimate is obtained as

$$\hat{u}[k]=\frac{\sum_{q=1}^{L}\hat{h}_q^*[k](h_q[k]u[k]+v_q[k])}{\sum_{a=1}^{L}\left|\hat{h}_a[k]\right|^2}$$
$$=u[k]\frac{\sum_{q=1}^{L}\hat{h}_q^*[k]h_q[k]}{\sum_{a=1}^{L}\left|\hat{h}_a[k]\right|^2}+\frac{\sum_{q=1}^{L}\hat{h}_q^*[k]v_q[k]}{\sum_{a=1}^{L}\left|\hat{h}_a[k]\right|^2} \tag{31}$$
$$=u[k]\frac{\sum_{q=1}^{L}\hat{h}_q^*[k]h_q[k]}{\sum_{a=1}^{L}\left|\hat{h}_a[k]\right|^2}+H[k].$$

The effective noise $H[k]$ is the weighted sum of the noise terms $v_q[k]$'s and is therefore a complex white random process with zero mean. When conditioned on the uplink gain estimates $\hat{h}_q[k]$'s, $H[k]$ is complex Gaussian distributed with variance

$$\sigma^2_{H[k]|\hat{h}_1[k],\hat{h}_2[k],\ldots,\hat{h}_L[k]}=\frac{1}{2}E\left[\left|\frac{\sum_{q=1}^{L}\hat{h}_q^*[k]v_q[k]}{\sum_{a=1}^{L}\left|\hat{h}_a[k]\right|^2}\right|^2\middle|\hat{h}_1[k],\hat{h}_2[k],\ldots,\hat{h}_L[k]\right]$$
$$=\sum_{q=1}^{L}\sum_{l=1}^{L}\frac{\hat{h}_q^*[k]\hat{h}_l[k]}{\left(\sum_{a=1}^{L}\left|\hat{h}_a[k]\right|^2\right)^2}\frac{1}{2}E\left[v_q[k]v_l^*[k]\right] \tag{32}$$
$$=\sum_{q=1}^{L}\sum_{l=1}^{L}\frac{\hat{h}_q^*[k]\hat{h}_l[k]}{\left(\sum_{a=1}^{L}\left|\hat{h}_a[k]\right|^2\right)^2}\sigma_v^2\delta(q-l)=\frac{\sum_{q=1}^{L}\left|\hat{h}_q[k]\right|^2}{\left(\sum_{a=1}^{L}\left|\hat{h}_a[k]\right|^2\right)^2}\sigma_v^2$$
$$=\sigma_v^2\Big/\sum_{a=1}^{L}\left|\hat{h}_a[k]\right|^2.$$

As per (30), from the CSI symbol estimates $\hat{u}[mN+(l-1)+D]$, $l=1,2,\ldots,L$, the base station recovers the feedback downlink gain estimates as

$$
\begin{aligned}
&\hat{g}_l[mN+(l-1)] \\
&= \sqrt{2\sigma_{\ddot{g}}^2}\hat{u}[mN+(l-1)+D] \\
&= \ddot{g}_l[mN+(l-1)]\frac{\sum_{q=1}^{L}\hat{h}_q^*[mN+(l-1)+D]h_q[mN+(l-1)+D]}{\sum_{a=1}^{L}\left|\hat{h}_a[mN+(l-1)+D]\right|^2} \\
&\quad + \sqrt{2\sigma_{\ddot{g}}^2}H[mN+(l-1)+D], \qquad l=1,2,\ldots,L.
\end{aligned} \tag{33}
$$

If uplink channel estimation is sufficiently accurate,

$$
\hat{h}_q[mN+(l-1)+D] \approx h_q[mN+(l-1)+D],\ q=1,2,\ldots,L,
$$

then the feedback downlink gain estimates can be approximated by

$$
\begin{aligned}
&\hat{g}_l[mN+(l-1)] \\
&\approx \ddot{g}_l[mN+(l-1)]\frac{\sum_{q=1}^{L}\left|h_q[mN+(l-1)+D]\right|^2}{\sum_{a=1}^{L}\left|h_a[mN+(l-1)+D]\right|^2} \\
&\quad + \sqrt{2\sigma_{\ddot{g}}^2}H[mN+(l-1)+D] \\
&= \ddot{g}_l[mN+(l-1)] + \sqrt{2\sigma_{\ddot{g}}^2}H[mN+(l-1)+D], \quad l=1,2,\ldots,L.
\end{aligned} \tag{34}
$$

In effect, analog feedback induces the white non-Gaussian noise term $\sqrt{2\sigma_{\ddot{g}}^2}H[mN+(l-1)+D]$, which has zero mean and variance $\frac{\sigma_g^2+\sigma_n^2}{L-1}\frac{\sigma_v^2}{\sigma_h^2}$ (see Appendix A). Note that this distortion diminishes with more base station antennas L and increasing uplink SNR σ_h^2/σ_v^2. We shall demonstrate the accuracy of the feedback downlink gain estimates using analog feedback in Section 3.3.

In downlink data transmission as depicted in Figure 3-1, a second layer of linear prediction is used to extrapolate from the feedback downlink gain estimates

$\hat{g}_l[mN+(l-1)]$'s the gain estimates $\hat{g}_l[k]$'s at the data symbol positions, which in turn are used to calculate the adaptive transmission weights $w_l[k]=\hat{g}_l^*[k]\Big/\sqrt{\sum_{a=1}^{L}|\hat{g}_a[k]|^2}$, $l=1,2,\ldots,L$, as per (16). It is assumed that the feedback delay T_{Fb} is known and compensated for when predicting the $\hat{g}_l[k]$'s. There are $F=N-L$ data symbols per downlink frame as shown in Figure 3-2. For notational convenience, we refer to a data block as the F data symbols at which the downlink gain estimates $\hat{g}_l[k]$'s are forecast from the same set of past feedback estimates. Since the decorrelation between the true downlink gain $g_l[k]$ and its estimate $\hat{g}_l[k]$ increases as the channel predictor forecasts further into the future [8], their correlation coefficient $\rho_{g\hat{g}}[k]$ decreases across a data block. Furthermore, $\rho_{g\hat{g}}[k]$ is periodic in discrete time k with a period of N. A proposal for dealing with this periodicity in channel estimation accuracy is presented in Section 4.2.

As indicated in Section 2.3, since the downlink gain estimates $\hat{g}_l[k]$'s are not perfectly accurate, the beamformed gain $G[k]=\sqrt{\sum_{l=1}^{L}|\hat{g}_l[k]|^2}+U[k]$ as per (17) is complex and causes a phase shift on the transmitted symbol $s[k]$. If this phase shift is relatively small, then coherent detection based directly on the received symbol is able to yield reasonable error performance, especially for those symbols at the start of the data block. But we adopt the more practical approach of conventional DD. Both conventional DD and multiple symbol differential detection (MSDD) have been considered, though it was found that the performance advantage achievable by MSDD is rather minimal, which

we shall demonstrate in Section 4.1. Note that the first symbol in each data block has to be coherently detected based directly on the received symbol since the phase of its beamformed gain is not continuous with the phase of the gain of the last symbol in the previous block.

Before concluding this section, we briefly review the topic of minimum mean square error (MMSE) linear prediction of the channel gains. For illustrative purpose, we assume the use of J^{th} order linear prediction filters, and the absence of feedback delay, i.e., $T_{Fb} = DT = 0$. Consider first the prediction of the downlink gains as shown in Figure 3-4. The downlink gain estimates $\hat{g}_l[k]$'s at the F data symbol positions in the m^{th} frame are given by [18], [19]

$$\begin{aligned} \hat{g}_l[k] = \mathbf{c}_l[k]\mathbf{d}_l, \;\; & l = 1,2,\ldots,L, \text{ and} \\ & k = mN + (L-1) + 1, mN + (L-1) + 2, \\ & \quad \ldots, mN + (L-1) + F, \end{aligned} \tag{35}$$

where $\mathbf{c}_l[k] = \left[c_l^{(J-1)}[k]\, c_l^{(J-2)}[k] \ldots c_l^{(0)}[k]\right]$ are the filter coefficients and $\mathbf{d}_l = [\hat{g}_l[(m-J+1)N + (l-1)]\, \hat{g}_l[(m-J+2)N + (l-1)] \ldots \hat{g}_l[mN + (l-1)]]^T$ are the J most recent feedback downlink gain estimates. Note that $(\cdot)^T$ denotes matrix transpose. The filter coefficients are determined according to

$$\mathbf{c}_l[k] = \boldsymbol{\varphi}_{gd,l}[k]\boldsymbol{\Phi}_{dd,l}^{-1}, \tag{36}$$

where $\boldsymbol{\Phi}_{dd,l} = \frac{1}{2}E\left[\mathbf{d}_l\mathbf{d}_l^H\right]$ is the autocorrelation matrix of $\mathbf{d}_l$, and $\boldsymbol{\varphi}_{gd,l}[k] = \frac{1}{2}E\left[g_l[k]\mathbf{d}_l^H\right]$ is the cross-correlation vector between $g_l[k]$ and $\mathbf{d}_l$. Note that $(\cdot)^H$ denotes Hermitian transpose. It can be shown that the correlation coefficient between the true downlink gain $g_l[k]$ and its estimate $\hat{g}_l[k]$ is

$$\rho_{g\hat{g},l}[k]=\sqrt{\frac{\boldsymbol{\varphi}_{gd,l}[k]\boldsymbol{\Phi}_{dd,l}^{-1}\boldsymbol{\varphi}_{dg,l}[k]}{\sigma_g^2}},\ l=1,2,\ldots,L,\ \text{and}\quad k=mN+(L-1)+1,mN+(L-1)+2,\ldots,mN+(L-1)+F. \tag{37}$$

For simplicity, we assume $\boldsymbol{\Phi}_{dd,l}$ and $\boldsymbol{\varphi}_{gd,l}[k]$ are known a priori, and the correlation coefficient is the same among all channels, i.e., $\rho_{g\hat{g},l}[k]=\rho_{g\hat{g}}[k]$. Note that if uplink channel estimation is accurate, it follows from (28) and (34) that the feedback downlink gain estimates are approximated by

$$\begin{aligned}&\hat{g}_l[mN+(l-1)]\\&=\ddot{g}_l[mN+(l-1)]+\sqrt{2\sigma_{\ddot{g}}^2}H[mN+(l-1)+D]\\&=g_l[mN+(l-1)]+n[mN+(l-1)]+\sqrt{2\sigma_{\ddot{g}}^2}H[mN+(l-1)+D],\ l=1,2,\ldots,L.\end{aligned}$$

Then from (6), the autocorrelation function of the feedback downlink gain estimates is

$$\begin{aligned}&\frac{1}{2}E\left[\hat{g}_l[mN+(l-1)]\hat{g}_l^*[mN+(l-1)-aN]\right]\\&=\sigma_g^2J_0(2\pi f_d aNT)+\left(\sigma_n^2+\frac{\sigma_g^2+\sigma_n^2}{L-1}\frac{\sigma_v^2}{\sigma_h^2}\right)\delta(aN),\ |a|=0,1,\ldots,J-1,\end{aligned} \tag{38}$$

and the cross-correlation function between the downlink gains at the data symbols and the past feedback estimates is

$$\begin{aligned}&\frac{1}{2}E\left[g_l[k]\hat{g}_l^*[mN+(l-1)-bN]\right]\\&=\sigma_g^2J_0(2\pi f_d(k-(mN+(l-1)-bN))T),\ b=0,1,\ldots,J-1.\end{aligned} \tag{39}$$

Using these expressions, we can determine the elements of $\boldsymbol{\Phi}_{dd,l}$ and $\boldsymbol{\varphi}_{gd,l}[k]$, and compute the filter coefficients $\mathbf{c}_l[k]$ and the correlation coefficient $\rho_{g\hat{g}}[k]$ as per (36) and (37), respectively.

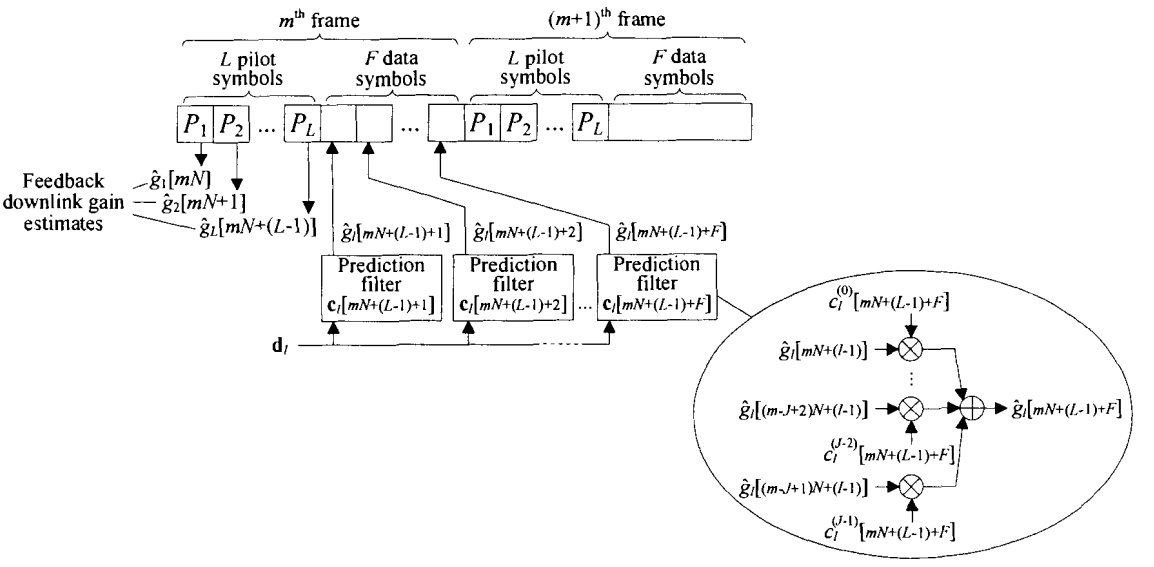

Figure 3-4. Linear prediction of downlink gains.

Linear prediction of the uplink gains, as shown in Figure 3-5, follows the same principles as the prediction of the downlink gains. We are primarily concerned with finding the uplink gain estimates $\hat{h}_q[k]$'s at the L feedback symbol positions in each frame, which in the m th frame are given by

$$\begin{aligned} \hat{h}_q[k] &= \mathbf{e}[k]\mathbf{f}_q, \quad q = 1,2,\ldots,L, \text{ and} \\ & \qquad k = mN+1, mN+2, \ldots, mN+L, \end{aligned} \tag{40}$$

where $\mathbf{f}_q = \left[\hat{h}_q[(m-J+1)N]\, \hat{h}_q[(m-J+2)N] \ldots \hat{h}_q[mN]\right]^T$ are the J most recent uplink gain estimates obtained from the pilot symbols, and $\mathbf{e}[k] = \left[e^{(J-1)}[k]\, e^{(J-2)}[k] \ldots e^{(0)}[k]\right]$ are the filter coefficients. The filter coefficients are determined according to

$$\mathbf{e}[k] = \boldsymbol{\varphi}_{hf}[k]\boldsymbol{\Phi}_{ff}^{-1} \tag{41}$$

where $\boldsymbol{\Phi}_{ff} = \frac{1}{2}E\left[\mathbf{f}_q\mathbf{f}_q^H\right]$ is the autocorrelation matrix of $\mathbf{f}_q$, and $\boldsymbol{\varphi}_{hf}[k] = \frac{1}{2}E\left[h_q[k]\mathbf{f}_q^H\right]$ is the cross-correlation vector between $h_q[k]$ and $\mathbf{f}_q$. Note that the same filter coefficients

can be used for all the channels since $\mathbf{\Phi}_{ff}$ and $\boldsymbol{\varphi}_{hf}[k]$ are the same among all channels. The elements of $\mathbf{\Phi}_{ff}$ and $\boldsymbol{\varphi}_{hf}[k]$ can be determined as follows. As per (29) the uplink gain estimates are obtained from the pilot symbols as

$$\hat{h}_q[mN] = h_q[mN] + v_q[mN],\ q = 1,2,\ldots,L\,.$$

Then from (24) the autocorrelation function of the pilot estimates is

$$\begin{aligned}&\frac{1}{2}E\left[\hat{h}_q[mN]\hat{h}_q^*[mN-aN]\right]\\&=\sigma_h^2 J_0(2\pi f_d aNT)+\sigma_v^2\delta(aN),\ |a|=0,1,\ldots,J-1,\end{aligned}\tag{42}$$

and the cross-correlation function between the uplink gains at the feedback symbols and the past pilot estimates is

$$\begin{aligned}&\frac{1}{2}E\left[h_q[k]\hat{h}_q^*[mN-bN]\right]\\&=\sigma_h^2 J_0(2\pi f_d(k-(mN-bN))T),\ b=0,1,\ldots,J-1.\end{aligned}\tag{43}$$

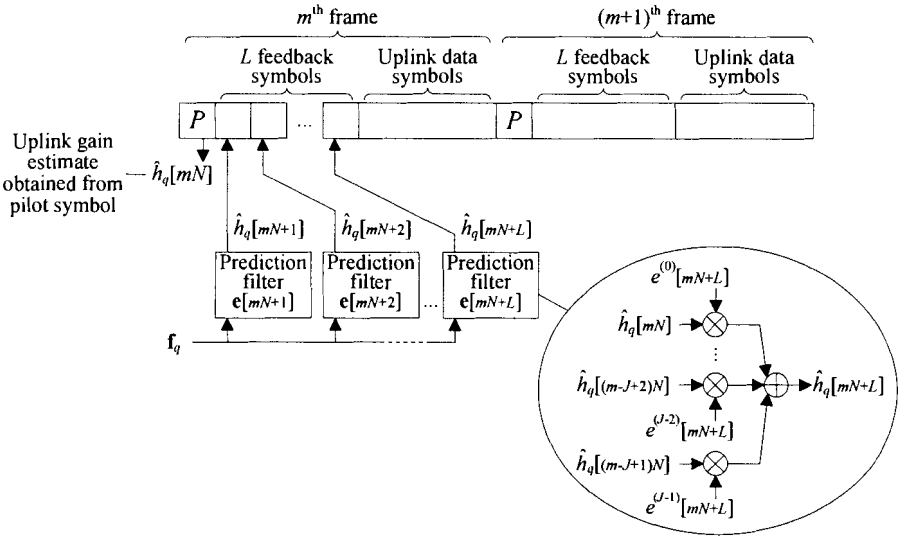

Figure 3-5. Linear prediction of uplink gains.

3.2 Digital CSI Feedback

To illustrate the effectiveness of the proposed analog feedback scheme, we compare it against digital feedback schemes that require the same average feedback rate. Downlink gain estimates are quantized and then fed back using one square QAM symbol per base station antenna per frame, or multiple PSK symbols – that are modulated using a smaller constellation – per base station antenna per frame. We emphasize that while the feedback schemes differ from that considered in the last section, downlink data transmission procedures remain the same and will not be reiterated here.

Consider first the use of one QAM feedback symbol per base station antenna per frame, where the timing between downlink channel estimation and CSI feedback is outlined in Figure 3-6 (a). As indicated in Section 2.5, pilot symbols are inserted into the downlink/uplink symbol stream between frames of T_{Fr} seconds, or N symbols, to facilitate periodic channel estimation. In each downlink frame, the downlink gain estimates $\ddot{g}_l[mN+(l-1)]$, $l=1,2,\ldots,L$, acquired by the mobile unit are digitized, mapped to L CSI symbols $u_1,u_2,\ldots,u_L$, and fed back to the base station at the start of the next uplink frame. To digitize each $\ddot{g}_l[mN+(l-1)]$, we encode its I-Q components into a pair of $x/2$-bit codewords using separate scalar quantizers[1]. The quantizer has $\sqrt{X}=2^{x/2}$ levels and is designed using the Lloyd algorithm (see Appendix B) to minimize the mean square error distortion

$$\begin{aligned}\varepsilon &= E\left[\left|\mathrm{Re}\{\tilde{g}_l[mN+(l-1)]\}-\mathrm{Re}\{\ddot{g}_l[mN+(l-1)]\}\right|^2\right] \\ &= E\left[\left|\mathrm{Im}\{\tilde{g}_l[mN+(l-1)]\}-\mathrm{Im}\{\ddot{g}_l[mN+(l-1)]\}\right|^2\right],\ l=1,2,\ldots,L,\end{aligned} \tag{44}$$

[1] While jointly encoding all L downlink gain estimates using a vector quantizer is more efficient, here we opt for separate encoding of the estimates using scalar quantizers to ensure that the quantized estimates remain statistically independent.

between $\ddot{g}_l[mN+(l-1)]$ and its quantized version $\tilde{g}_l[mN+(l-1)]$, where Re{·} and Im{·} are the real and imaginary parts of a complex number, respectively. Altogether the quantized downlink gain estimate $\tilde{g}_l[mN+(l-1)]$ is represented by an x-bit codeword, which is Gray mapped to the square QAM symbol u_l with constellation size $X = 2^x$. Similar to analog feedback, we assume a feedback delay of T_{Fb} seconds equal to D symbol intervals, where $D \geq L$. Therefore, the digital CSI symbols u_l's can be expressed as uplink symbols as $u[mN+(l-1)+D]$, $l = 1,2,\ldots,L$.

Transmission of the CSI symbol $u[k]$ in the uplink is modelled in Figure 3-6 (b). Periodic uplink gain estimates $\hat{h}_q[mN]$, $q = 1,2,\ldots,L$, obtained from the pilot symbols are used to extrapolate the gain estimates $\hat{h}_q[k]$'s at the data symbol positions, which in turn are used to perform MRC of the received symbols and amplitude fading compensation. The resultant symbol is then used as the decision variable for detecting the CSI symbol estimate $\hat{u}[k]$. From the CSI symbol estimates $\hat{u}[mN+(l-1)+D]$, $l = 1,2,\ldots,L$, the base station recovers the feedback downlink gain estimates as $\hat{g}_l[mN+(l-1)]$, $l = 1,2,\ldots,L$. Obviously, if $\hat{u}[mN+(l-1)+D]$ is detected in error, then $\hat{g}_l[mN+(l-1)]$ can be substantially different from the intended value of $\tilde{g}_l[mN+(l-1)]$. Even if $\hat{u}[mN+(l-1)+D]$ is detected correctly, the quantization error ε inherent in $\hat{g}_l[mN+(l-1)]$ remains. We shall demonstrate the accuracy of the feedback downlink gain estimates using digital feedback in Section 3.3.

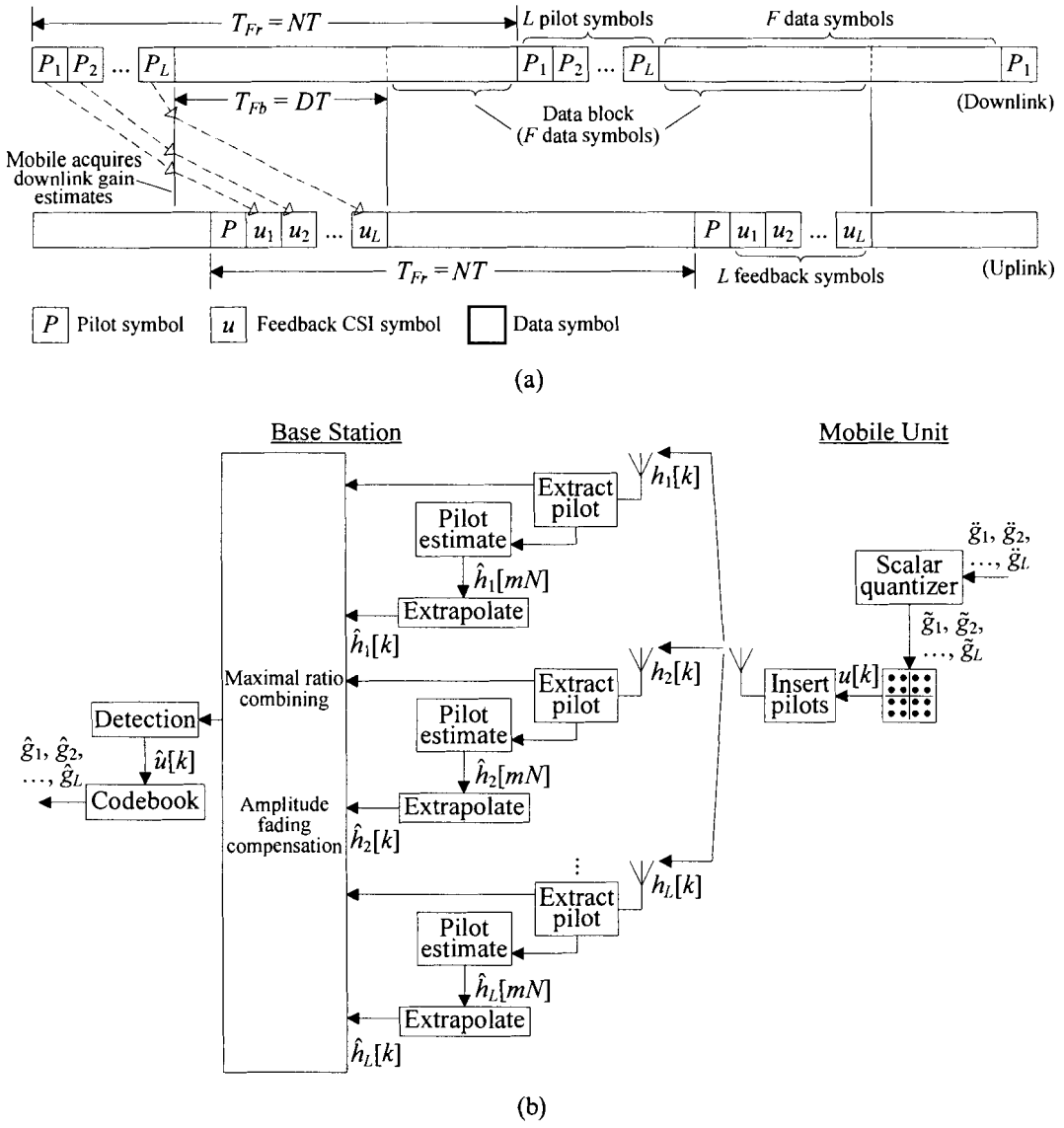

Figure 3-6. Closed-loop system using QAM symbols for CSI feedback. (a) Data frame structure. (b) Uplink model.

In the preceding discussion, we use one digital feedback symbol per base station antenna per frame as in the analog feedback scheme. A natural question is whether it is beneficial to use multiple digital feedback symbols that are modulated using a smaller constellation per base station antenna per frame, and thereby lower the probability of feedback error. To answer this question, we also try feeding back the x-bit codeword of each quantized downlink gain estimate $\tilde{g}_l[mN + (l-1)]$ using two PSK symbols $u_{l,1}$ and

$u_{l,2}$ with constellation size $\sqrt{X} = 2^{x/2}$, as exemplified in Figure 3-7. When using one QAM symbol per base station antenna per frame, the average feedback rate is L/N. On the other hand, when using two PSK symbols per base station antenna per frame, the total number of feedback symbols is doubled. In order to maintain the same average feedback rate for fair comparison, we extend the frame duration to T'_{Fr} seconds equal to $2N$ symbol intervals yielding an average feedback rate of $2L/2N \equiv L/N$. Certainly, the Nyquist sampling criterion must be satisfied, so for this approach to be feasible it is required that $1/T'_{Fr} = 1/2NT \geq 2f_d$.

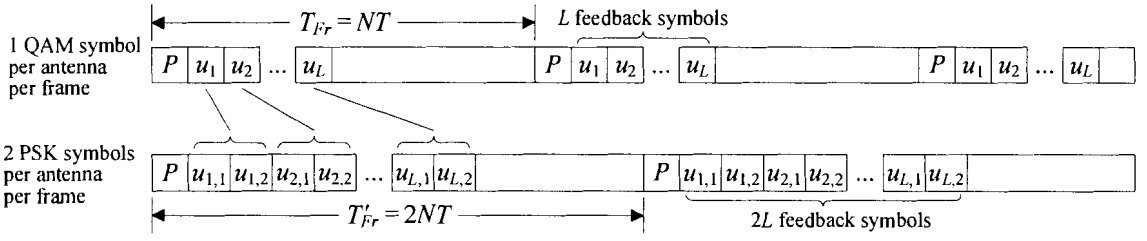

Figure 3-7. Uplink data frame structure using one QAM symbol vs. two PSK symbols per base station antenna per frame.

The revised timing between downlink channel estimation and CSI feedback is shown in Figure 3-8 (a). Since a longer transmission time is needed where there are more feedback symbols, we assume a feedback delay of T'_{Fb} seconds equal to D' symbol intervals, where $D' \geq 2L$. Transmission of the CSI symbol $u[k]$ in the uplink is shown in Figure 3-8 (b), which only differ from using one feedback symbol per base station antenna per frame (see Figure 3-6 (b)) in that periodic uplink gain estimates $\hat{h}_q[m(2N)]$, $q = 1,2,\ldots,L$, are obtained from pilots spaced every $2N$ symbol intervals. Note that in downlink data transmission, since the frame size is extended to $2N$ symbols, there are

$N+F=2N-L$ data symbols per downlink frame (see Figure 3-8 (a)). As indicated in the last section, downlink gain estimates are less accurate at symbols further away from the start of the data block. All things considered, feedback is more accurate but less timely when using more digital CSI symbols per channel per frame, and the overall downlink performance may actually be worse (see also [10]). We shall demonstrate the impact of this trade off between feedback accuracy and timeliness in Section 3.3.

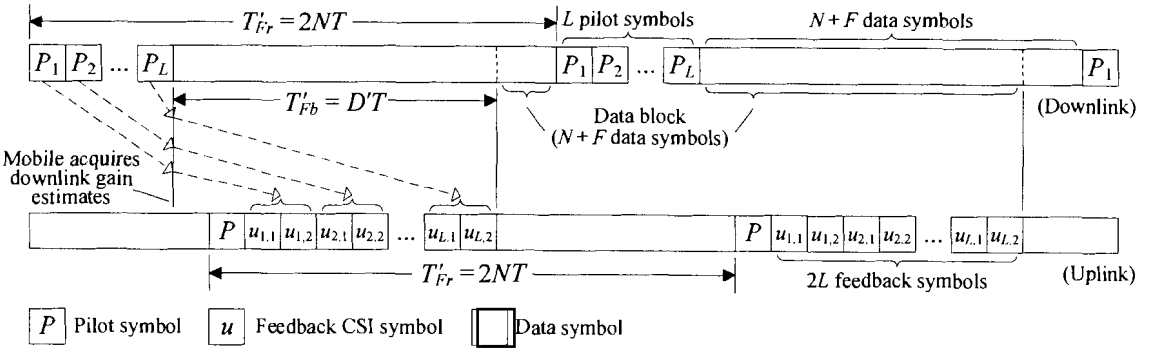

(a)

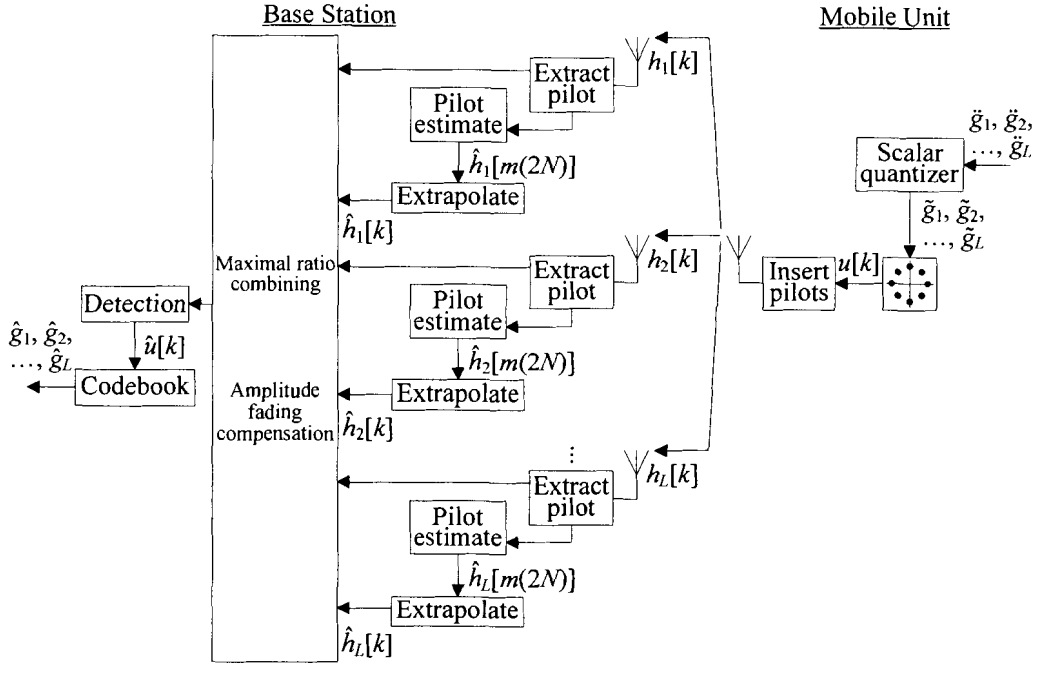

(b)

Figure 3-8. Closed-loop system using PSK symbols for CSI feedback. (a) Data frame structure. (b) Uplink model.

3.3 Simulation Results and Discussions

This section presents the simulated downlink error rates of the proposed closed-loop system. For the purpose of illustration, we consider simulations defined by the parameters listed in Table 3-1. We assume the base station is equipped with 4 or 3 antennas, the fading channels vary slowly in time with normalized Doppler frequencies of $f_d T = 0.002$ and $f_d T = 0.005$, and the frame size is chosen such that the channel estimation rate is approximately 4 or 6 times the Doppler frequency f_d. For simplicity, we focus on the downlink performance with a minimal feedback delay that equals to the transmission time of the CSI symbols. In this case, the delay of D symbol intervals is much smaller than the channel coherence time of $1/f_d$. Moreover, we assume that the base station performs linear channel prediction with the $J = 10$ most recent pilot estimates, for extrapolating uplink gains used to detect feedback CSI symbols, and for extrapolating downlink gains used to calculate adaptive transmission weights.

To help interpret the simulation results, we list in Table 3-2 the equivalent mobile speeds and feedback rates under typical conditions. For instance, if the carrier frequency is 1.9 GHz and the baud rate is 30 kHz, then normalized Doppler frequencies of $f_d T = 0.002$ and $f_d T = 0.005$ correspond to mobile speeds of approximately 35 km/hr and 85 km/hr, respectively. Furthermore, if the base station is equipped with 4 antennas and the mobile is moving at 35 km/hr, then periodic channel estimation at 6 times the Doppler frequency requires a feedback rate of approximately 1450 symbols per second (sps).

Table 3-1. Simulation parameters.

Base antennas L	Normalized Doppler frequency f_dT	Channel coherence time $1/f_d$	Channel estimation rate (approx.) $1/T_{Fr}$, $T_{Fr} = NT$	Frame size N	Feedback delay D	Prediction filter order J
4	0.002	$500T$	$4f_d$	128	4	10
			$6f_d$	84		
	0.005	$200T$	$4f_d$	52		
			$6f_d$	36		
3	0.002	$500T$	$4f_d$	127	3	
			$6f_d$	83		
	0.005	$200T$	$4f_d$	51		
			$6f_d$	35		

Table 3-2. Mobile speeds and feedback rates in the simulations.

Base antennas L	Carrier frequency	Baud rate $1/T$	Normalized Doppler freq. f_dT	Mobile speed (approx.)	Channel estimation rate (approx.) $1/T_{Fr}$	Feedback rate (approx.)
4	1.9 GHz	30 kHz	0.002	35 km/hr	$4f_d$	950 sps
					$6f_d$	1450 sps
			0.005	85 km/hr	$4f_d$	2300 sps
					$6f_d$	3350 sps
3			0.002	35 km/hr	$4f_d$	700 sps
					$6f_d$	1100 sps
			0.005	85 km/hr	$4f_d$	1750 sps
					$6f_d$	2550 sps

We consider first the accuracy of the feedback CSI in order to highlight the different behaviors among the proposed analog feedback scheme and its digital feedback counterparts. To quantify feedback accuracy, we measure the feedback CSI SNR defined as

$$\frac{\frac{1}{2}E\left[\left|g_l[mN+(l-1)]\right|^2\right]}{\frac{1}{2}E\left[\left|\hat{g}_l[mN+(l-1)]-g_l[mN+(l-1)]\right|^2\right]} = \frac{\sigma_g^2}{\frac{1}{2}E\left[\left|\hat{g}_l[mN+(l-1)]-g_l[mN+(l-1)]\right|^2\right]}, \quad l=1,2,\ldots,L, \tag{45}$$

where $\hat{g}_l[mN+(l-1)]$ is the feedback downlink gain estimate recovered by the base station and $g_l[mN+(l-1)]$ is the true gain. It was found that the CSI SNR is approximately the same for all channels. However, it should be understood that the distortion in the feedback CSI, i.e., $\frac{1}{2}E\left[\left|\hat{g}_l[mN+(l-1)]-g_l[mN+(l-1)]\right|^2\right]$, can be slightly different for each channel. This is because the feedback CSI symbols u_l's for the individual channels are transmitted at different positions in the uplink frame (e.g., see Figure 3-2), and the $\hat{g}_l[mN+(l-1)]$'s are obtained from the u_l's using uplink gain estimates of different accuracy that are extrapolated via linear prediction.

In Figure 3-9 to Figure 3-12, we show some performance curves using analog feedback and digital feedback with 2- or 4-bit quantization of the downlink gain estimates. As indicated in Section 3.2, we feed back a 2-bit CSI codeword using one 4QAM symbol or two BPSK symbols, and feed back a 4-bit CSI codeword using one 16QAM symbol or two QPSK symbols. We reiterate that when using two feedback symbols per base station antenna per frame, the frame size is doubled to maintain the same average feedback rate, and the feedback delay is set twice as long to reflect the longer transmission time needed by more feedback symbols.

We compare in part (a) of Figure 3-9 to Figure 3-12 the feedback CSI SNR using different feedback schemes. From the curves of analog feedback, as predicted by (34), it can be seen that the feedback CSI SNR continuously improves with increasing symbol SNR. On the contrary, from the curves of digital feedback, it can be seen that the feedback CSI SNR levels off at high symbol SNR because of unrecoverable quantization error. The amount of unrecoverable error can be lessened by quantizing the downlink gain estimates with higher precision, but the resultant feedback symbols are modulated using a larger constellation, and so the probability of feedback error is higher. Therefore, unlike analog feedback, the effectiveness of digital feedback is affected by the difficult trade off between quantization and feedback errors. As expected, feedback error is reduced by using more feedback symbols, but this advantage becomes less valuable with increasing symbol SNR as quantization error begins to dominate.

We compare in part (b) of Figure 3-9 to Figure 3-12 the downlink BER of differential BPSK using different feedback schemes. Since more accurate feedback CSI leads to more effective beamforming and subsequently better BER performance, the BER curves of digital feedback using 2- and 4-bit quantization cross at approximately the symbol SNR where the CSI SNR curves cross. Furthermore, since the analog feedback scheme is free of quantization error, it achieves better CSI accuracy and BER performance than the digital feedback schemes. Although the use of two PSK feedback symbols per base station antenna per frame reduces feedback error, it degrades the average BER. This is because, in order to maintain the same feedback rate, there are more data symbols per downlink frame in the two feedback symbols case, and those symbols further into the future from the start of the data block have significantly worse

error performance. All things considered, these results suggest that analog feedback is superior to digital feedback under the same operating conditions. For reference, we also show the BER curve for the ideal case that transmission weights are calculated from perfectly accurate CSI[2], as well as the BER curve for error and delay free periodic feedback CSI. Note that with error and delay free feedback CSI, linear prediction is still required to obtain downlink gain estimates for calculating adaptive transmission weights, and performance is affected by the prediction error in the downlink gain estimates. On the other hand, note that the slope of the BER curve for analog feedback and is very similar to that of error and delay free feedback CSI, which implies that analog feedback can achieve similar diversity gain as error and delay free feedback CSI.

[2] Note that with perfect CSI, as per (11), the beamformed gain $G[k]$ is real and data is detected coherently based directly on the received symbol.

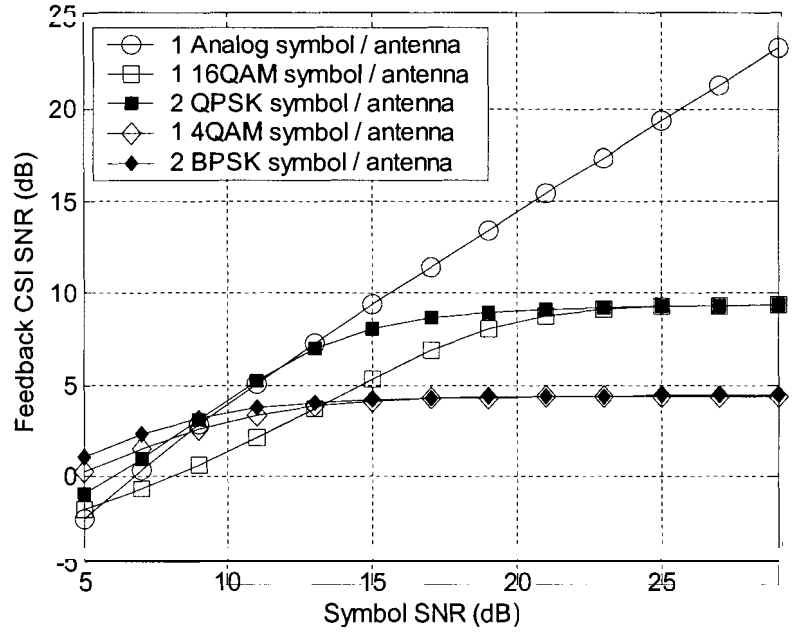

(a)

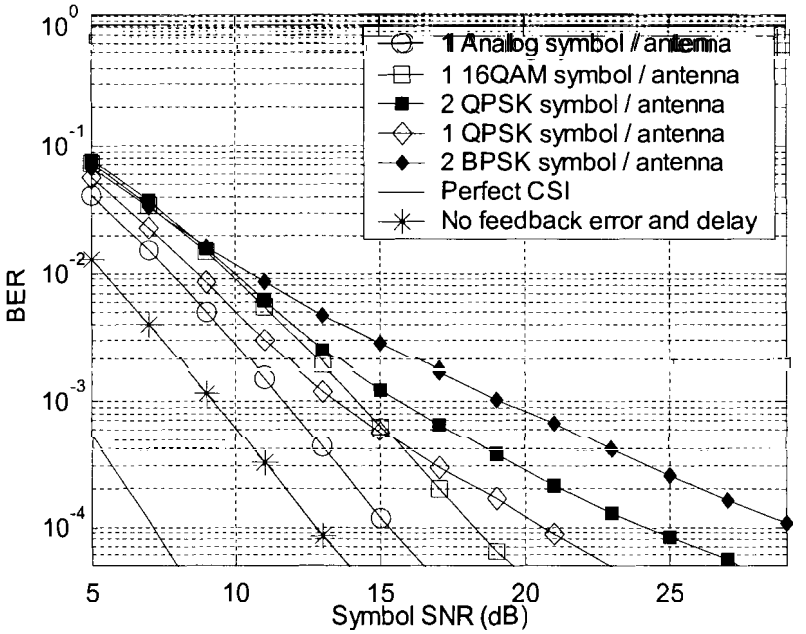

(b)

Figure 3-9. **(a) Feedback CSI SNR and (b) BER of differential BPSK using analog and digital feedback; $f_dT = 0.002$ and $L = 4$.**
Using one feedback symbol per base station antenna per frame, $N = 84$ and $D = 4$.
Using two feedback symbols per base station antenna per frame, $N = 168$ and $D' = 8$.

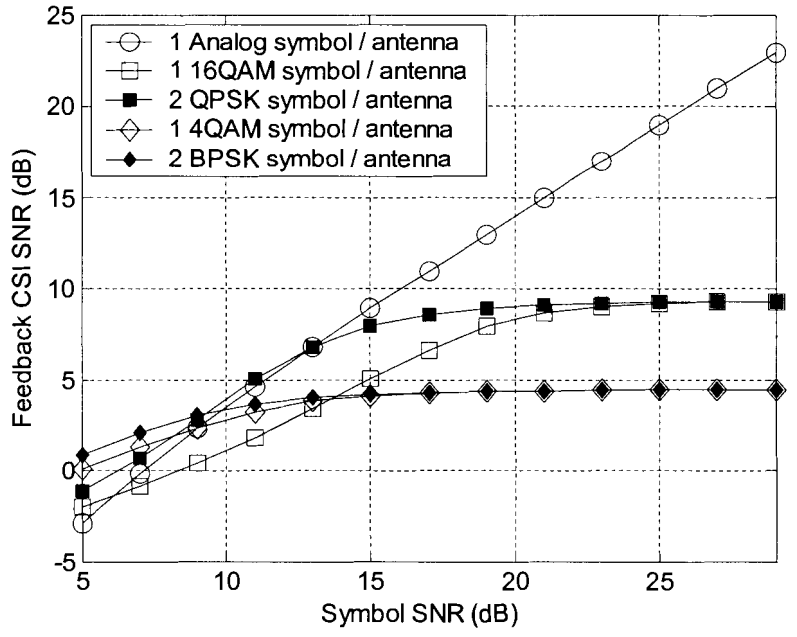

(a)

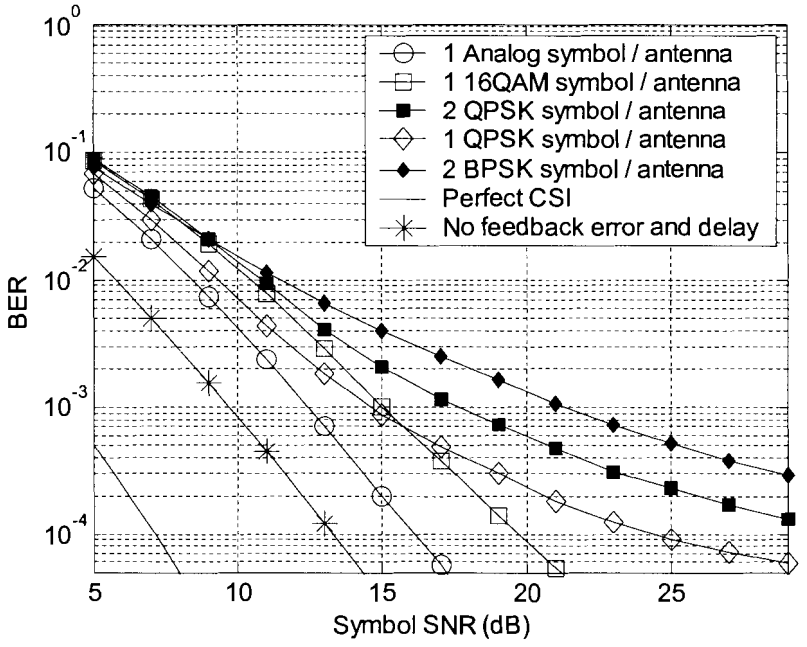

(b)

Figure 3-10. (a) Feedback CSI SNR and (b) BER of differential BPSK using analog and digital feedback; $f_dT = 0.005$ and $L = 4$.
Using one feedback symbol per base station antenna per frame, $N = 36$ and $D = 4$.
Using two feedback symbols per base station antenna per frame, $N = 72$ and $D' = 8$.

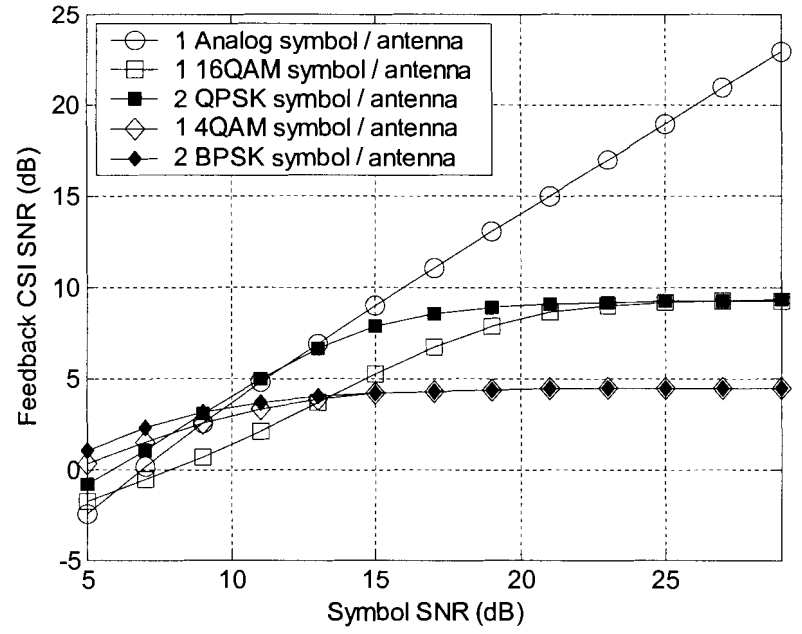

(a)

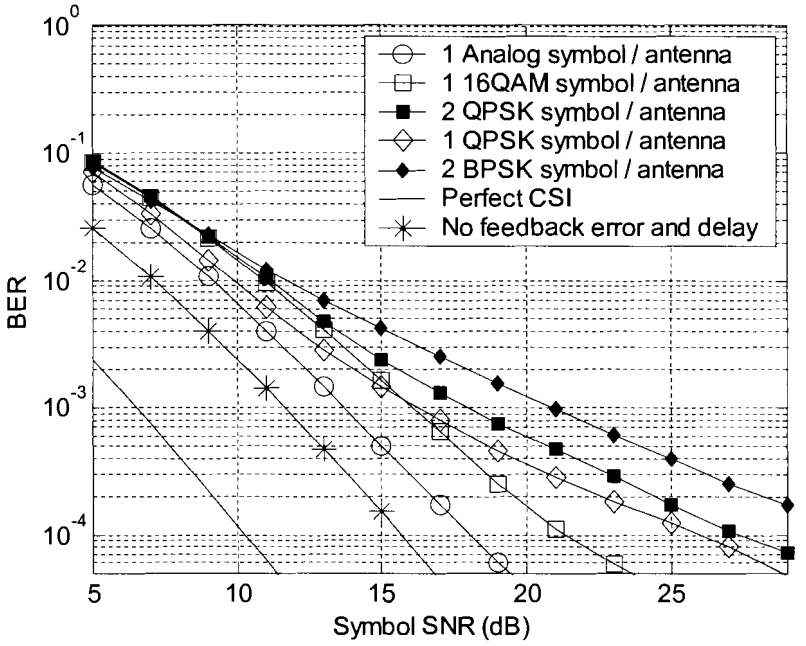

(b)

Figure 3-11. (a) Feedback CSI SNR and (b) BER of differential BPSK using analog and digital feedback; $f_dT = 0.002$ and $L = 3$.
Using one feedback symbol per base station antenna per frame, $N = 83$ and $D = 3$.
Using two feedback symbols per base station antenna per frame, $N = 166$ and $D' = 6$.

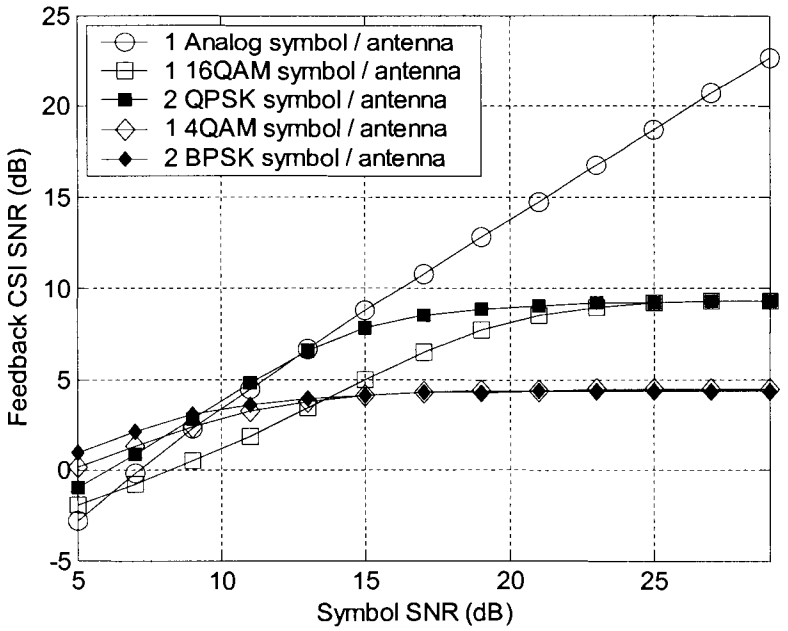

(a)

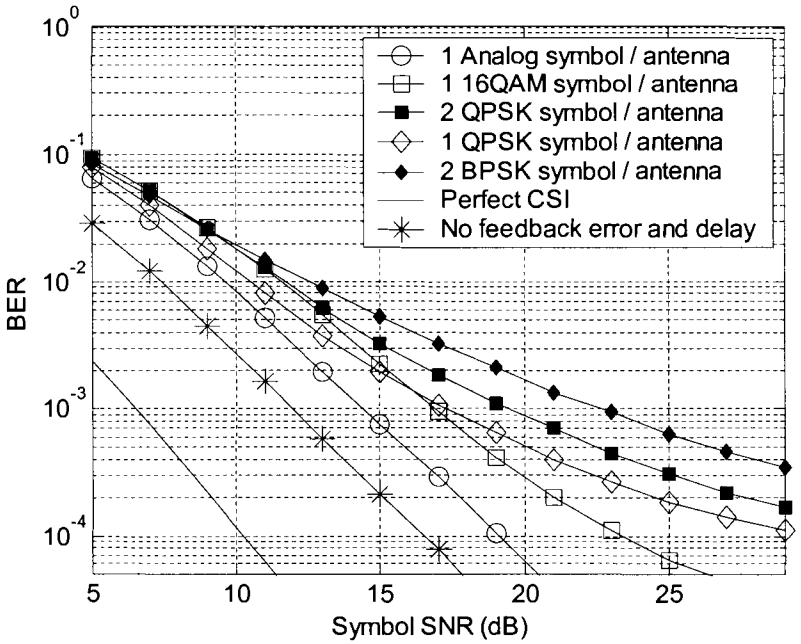

(b)

Figure 3-12. (a) Feedback CSI SNR and (b) BER of differential BPSK using analog and digital feedback; $f_dT = 0.005$ and $L = 3$.
Using one feedback symbol per base station antenna per frame, $N = 35$ and $D = 3$.
Using two feedback symbols per base station antenna per frame, $N = 70$ and $D' = 6$.

To demonstrate the performance of the proposed closed-loop system under different operating conditions, we show in Figure 3-13 to Figure 3-16 the downlink BER curves of different modulations and different frame sizes. For reference, we also include the BER curves of digital feedback using one 16QAM symbol per base station antenna per frame. We have considered digital feedback using 4QAM, 16QAM and 64QAM symbols, and the use of 16QAM feedback symbols is found to perform the best over a wide range of SNR.

It can be seen that analog feedback provides an SNR advantage over digital feedback, and the BER curves have steeper slopes implying better diversity gain. In addition, note that the slopes of the BER curves using digital feedback flatten out quickly with increasing SNR. This performance loss is due to our use of conventional DD, which exhibits an error floor at high SNR. However, the BER curves using analog feedback do not show error floors. This is because analog feedback allows CSI accuracy and thus the effectiveness of beamforming to improve with SNR. It follows that, at high SNR, the beamformed gain has a strong direct component (and a weak diffuse component) such that the phase shift it imposes on the transmitted symbol diminishes, and the deficiency of conventional DD to account for a small phase shift has little impact on the BER performance.

Note that BER performance improves with shorter frame sizes because of the increased channel estimation rate (see Table 3-1 and Table 3-2), as well as the avoidance of more error prone symbols at the end of a long data block. However, since feedback rates are higher and pilots are transmitted more frequently, throughput is also affected. We shall discuss the various impacts of different frame sizes throughout Chapter 4.

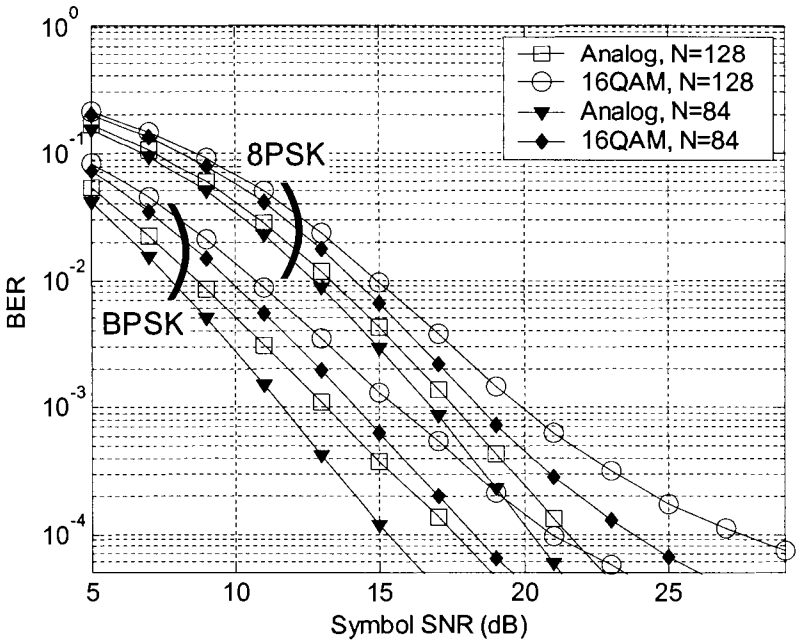

Figure 3-13. Bit error rate of differential BPSK and 8PSK using analog and digital feedback; $f_dT = 0.002$, $L = 4$, and $D = 4$.

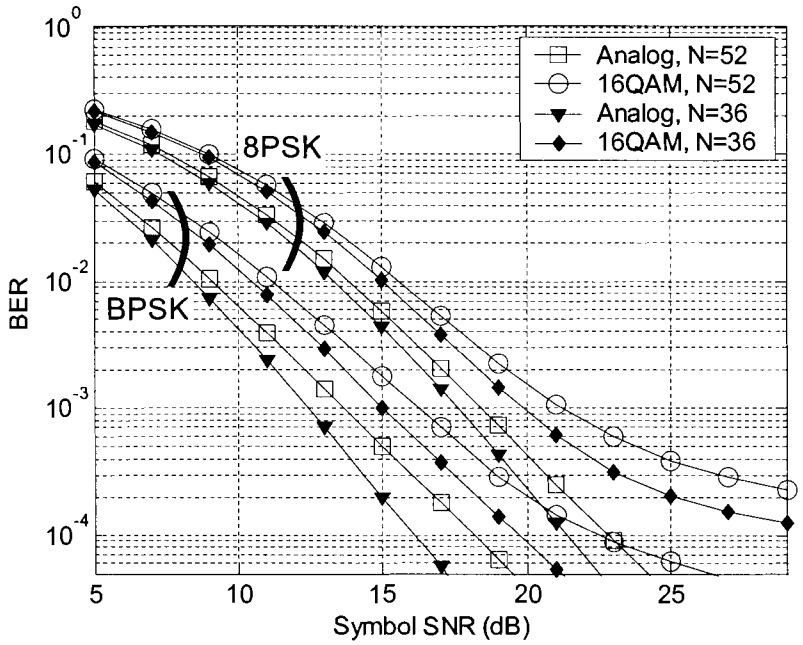

Figure 3-14. Bit error rate of differential BPSK and 8PSK using analog and digital feedback; $f_dT = 0.005$, $L = 4$, and $D = 4$.

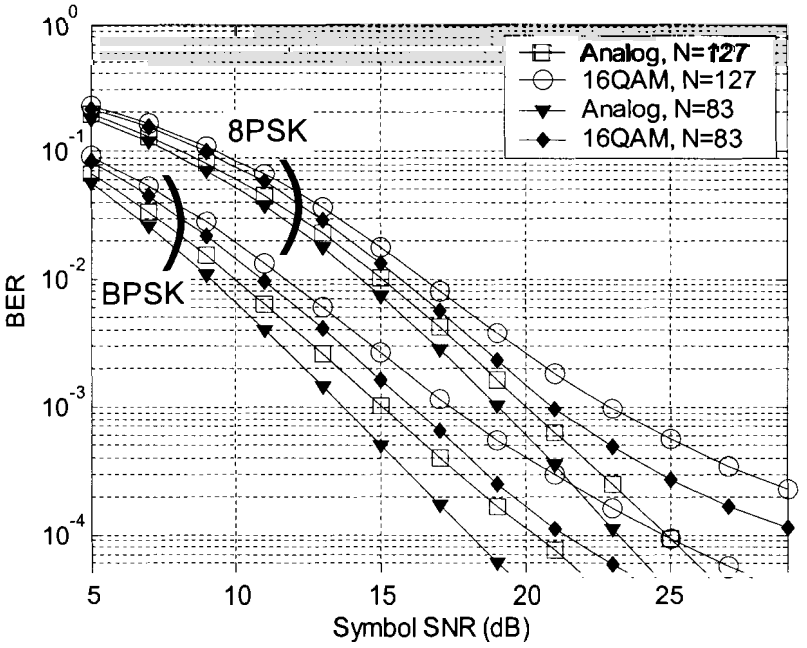

Figure 3-15. Bit error rate of differential BPSK and 8PSK using analog and digital feedback; $f_dT = 0.002$, $L = 3$, and $D = 3$.

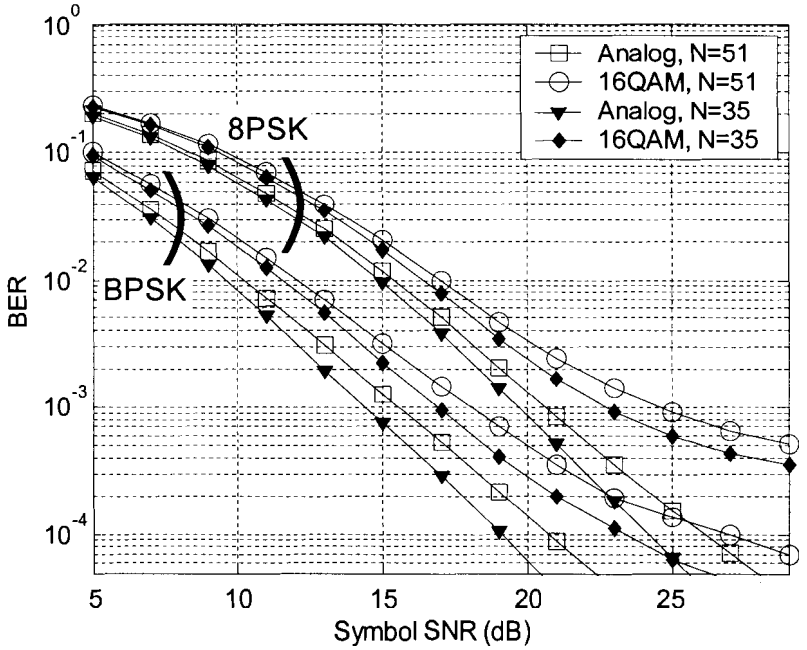

Figure 3-16. Bit error rate of differential BPSK and 8PSK using analog and digital feedback; $f_dT = 0.005$, $L = 3$, and $D = 3$.

3.4 Summary

We proposed in this chapter a closed-loop transmit diversity system that is based on an analog CSI feedback scheme. Downlink complex gains are periodically estimated at the mobile unit, and then fed back to the base station at a rate of only one analog symbol per estimate per data frame. Furthermore, between periodic feedback CSI updates, the base station performs linear channel prediction, and thereby calculates adaptive transmission weights for beamforming. To illustrate the effectiveness of the proposed analog feedback scheme, we compared it against digital feedback schemes that require the same average feedback rate. The performances of the different feedback schemes are evaluated in terms of feedback CSI accuracy and downlink BER. It was found that since digital feedback involves quantization, it causes unrecoverable distortion in the feedback CSI. In addition, at the given feedback rate, digital feedback must trade off between quantization and feedback errors. On the contrary, analog feedback does not involve quantization and thus allows CSI accuracy to improve continuously with SNR. Consequently, analog feedback always outperforms digital feedback under the same operating conditions.

CHAPTER 4 ASSOCIATED ISSUES WITH THE PROPOSED CLOSED-LOOP TRANSMIT DIVERSITY SYSTEM

The proposed closed-loop transmit diversity system based on analog feedback has significant performance advantages over implementations based on digital feedback. To further enhance performance and verify feasibility of the proposed system, here we investigate various associated issues and provide solutions. Specifically, we assess the performance gain of sequence detection, deal with the periodic variation in CSI accuracy and feedback delay that are natural to closed-loop systems, and study the dynamic range requirement of the mobile transmitter to implement analog feedback.

This chapter is organized as follows. We quantify the potential gain by employing multiple symbol differential detection (MSDD) in the downlink in Section 4.1. Next we present a variable rate position dependent modulation scheme to counter the periodic variation in CSI accuracy in Section 4.2. Then we discuss the impacts of feedback delay and frame size in Section 4.3. We present a simple modification to the analog feedback scheme for limiting the dynamic range of the feedback symbols in Section 4.4, followed by a chapter summary in Section 4.5.

4.1 Conventional DD vs. MSDD

As indicated in Section 3.1, we employ conventional 2-symbol differential detection (DD) in the downlink of the proposed closed-loop system. It is well known that MSDD can achieve better BER performance, which improves with the observed

sequence length, and approaches that of coherent detection of differentially encoded symbols [22]. To investigate the potential of MSDD in the proposed analog feedback closed-loop transmit diversity system, we compare in Figure 4-1 the downlink BER curves using conventional DD and coherent detection with differential encoding. The simulations are defined by the parameters listed in Table 3-1. Based on the results in Figure 4-1, we rule out the use of MSDD because it requires considerably greater computational complexity than conventional DD, but gives at best a 1 dB SNR gain for differential BPSK, and a 2 dB SNR gain for differential 8PSK. Such minor SNR gain is attributable to the beamformed gain having a strong direct component.

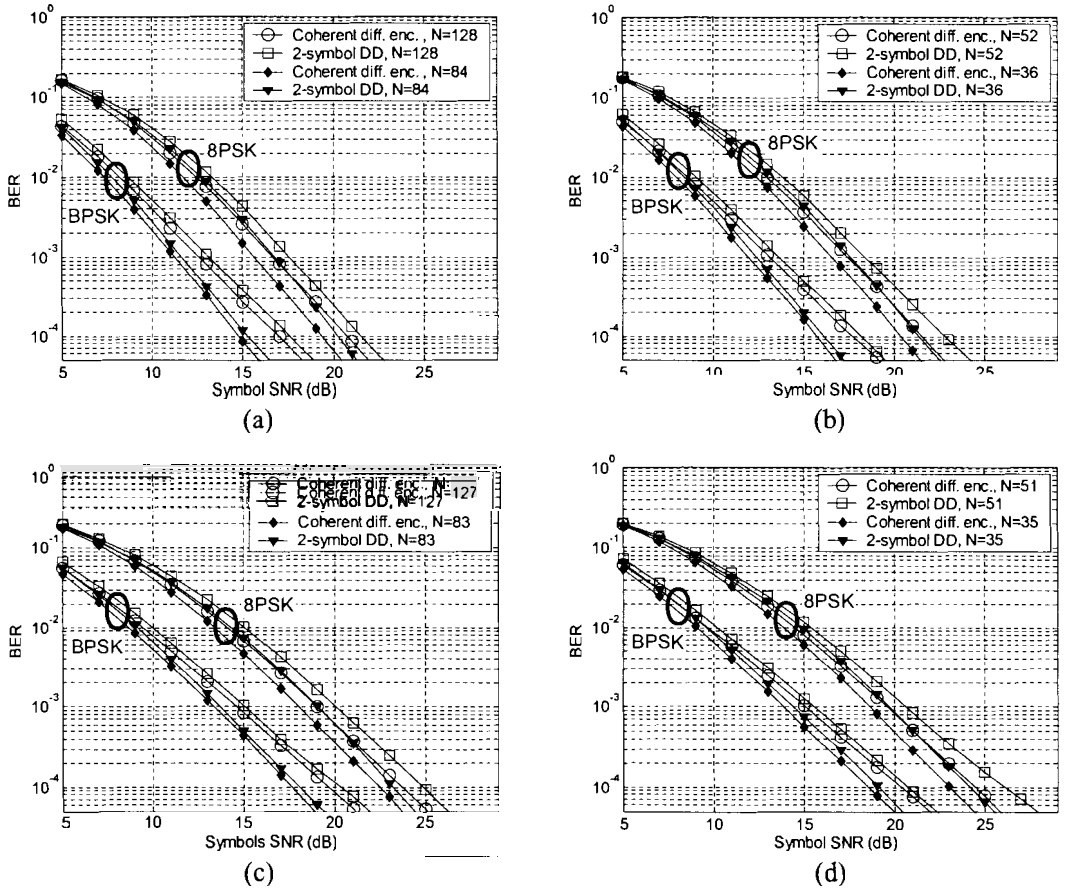

Figure 4-1. Bit error rate of differential BPSK and 8PSK using analog feedback; conventional DD and coherent detection with differential encoding.
(a) $f_dT = 0.002$, $L = 4$, and $D = 4$, (b) $f_dT = 0.005$, $L = 4$, and $D = 4$, (c) $f_dT = 0.002$, $L = 3$, and $D = 3$, and (d) $f_dT = 0.005$, $L = 3$, and $D = 3$.

4.2 Position Dependent Modulation

In practical closed-loop systems, the feedback rate is much lower than the baud rate, and so the mismatch between the feedback CSI and the channel conditions worsens significantly over the feedback period. As mentioned in Section 3.1, even with channel prediction in the proposed system, downlink gain estimates are less accurate at symbols further away from the start of the data block. Consequently, the effectiveness of beamforming, e.g., the detection SNR as per (19) and (20), is very different across the downlink frame.

Due to the impact of periodic variation in CSI accuracy, it is clearly inefficient to use the same modulation in every data symbol position of a downlink frame. This motivates the adoption of position dependent modulation (PDM), whereby the modulation used in each data symbol position in the frame is chosen in such a way that the downlink throughput is maximized for a target BER. The concept is similar to adaptive modulation[3] [9], though PDM is based on the statistical average of the SNR rather than the instantaneous SNR. We explain below the design procedure of a PDM scheme to be used in the proposed closed-loop system. Note that the design of PDM, in principle, need only be done once and offline, as it is not a real-time optimization process operating on the instantaneous SNR.

Again as indicated in Section 3.1, there are F data symbols per downlink frame. Let $P_{b,f}$, $f = 1,2,\ldots,F$, denote the BER's at the different symbol positions at the design

[3] We have also considered and ruled out adaptive modulation. With adaptive modulation, if the modulation switching rate is to be the same as the symbol rate, then CSI feedback must be error free; otherwise, the base station and the mobile unit will end up choosing different modulations, and data will always be detected in error.

SNR, where the symbol in the f^{th} position is modulated using a PSK constellation of size M_f and contains $B_f = \log_2 M_f$ bits per symbol. It follows that the throughput per downlink frame is $\sum_{a=1}^{F} B_a$, the average number of bits in error is $\sum_{f=1}^{F} B_f P_{b,f}$, and the average BER over the downlink frame is $\sum_{f=1}^{F} B_f P_{b,f} \Big/ \sum_{a=1}^{F} B_a$. Our objective is to find the optimal set of constellation sizes M_f's, such that the throughput is maximized at the target BER of BER_{Tgt}, i.e., solving the integer constrained resource allocation problem (see also [20 Section 8.4])

$$\begin{aligned} \max \quad & \sum_{a=1}^{F} B_a , \\ \text{subject to} \quad & BER_{Tgt} \geq \frac{\sum_{f=1}^{F} B_f P_{b,f}}{\sum_{a=1}^{F} B_a} . \end{aligned} \tag{46}$$

Equation (46) can be solved heuristically using a greedy algorithm [24 Ch. 16]. The idea is simple and intuitive. Starting with the initial choices of M_f's, the algorithm iteratively increases the throughput by a fixed number of bits by changing the modulation used in one symbol position at a time, until the average BER reaches BER_{Tgt}. The locally optimal choice of the symbol position to be adjusted at each iteration of the algorithm, clearly, is the one whose BER is least degraded due to the change.

The flow chart of the design of PDM is shown in Figure 4-2. We assume constellation size options of $M_f = \{2,4,8,16\}$ are available. Since the algorithm does not revise previous decisions, a reliable initial choice is $M_f = 2$ for every symbol position in

the frame. Bearing the objective is to increase the throughput by one bit at each iteration of the algorithm, the symbol in the i^{th} position is modulated using the next larger constellation, where the i^{th} position is chosen according to $\min_i\left(P_{b,i}^{new} - P_{b,i}\right)$, and $P_{b,i}^{new}$ denotes the BER after the modulation is changed. It follows that the final set of M_f's chosen as described above is globally optimal since no other combination of constellation sizes can achieve a higher throughput, or the same throughput with lower average BER over the downlink frame.

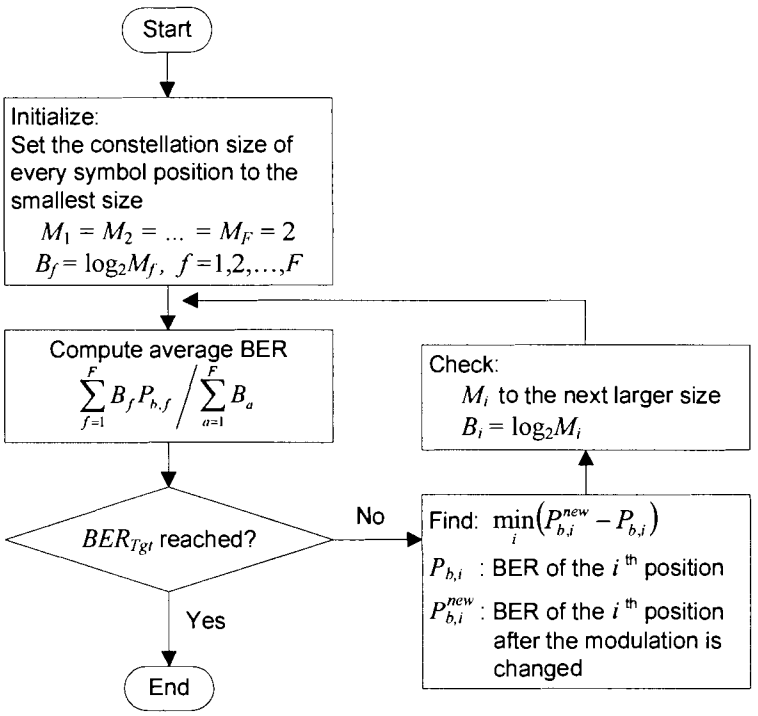

Figure 4-2. Flow chart of the design of PDM.

If the periodic variation in CSI accuracy is neglected, and every symbol in the downlink frame is modulated using the same PSK constellation of size M, then the throughput per frame is $\sum_{a=1}^{F} B_a = F \log_2 M$, and the average BER over the frame is

$\frac{1}{F}\sum_{f=1}^{F} P_{b,f}$. It follows that in order to maximize the throughput at the target BER of BER_{Tgt}, we would seek the Optimal Fixed Modulation (OFM) with constellation size M according to $\max_{M}\left(BER_{Tgt} \geq \frac{1}{F}\sum_{f=1}^{F} P_{b,f} \right)$. Obviously, OFM does not guarantee optimal throughput when the BER's of different symbol positions are significantly different.

To demonstrate the advantage of PDM over OFM, in Figure 4-3 and Figure 4-4 we compare the simulated throughput curves of the proposed closed-loop system at a target BER of $BER_{Tgt} = 10^{-3}$. The simulations are defined by the parameters listed in Table 3-1. As expected, it can be seen that PDM yields substantially higher throughput than OFM. Note that at low SNR, the target BER may not be satisfied even if every symbol is BPSK modulated, e.g., below 15 dB SNR in Figure 4-3 (a). On the contrary, at high SNR, the target BER is satisfied even if every symbol is 16PSK modulated, and so the throughput levels off, e.g., beyond 23 dB SNR in Figure 4-3 (a).

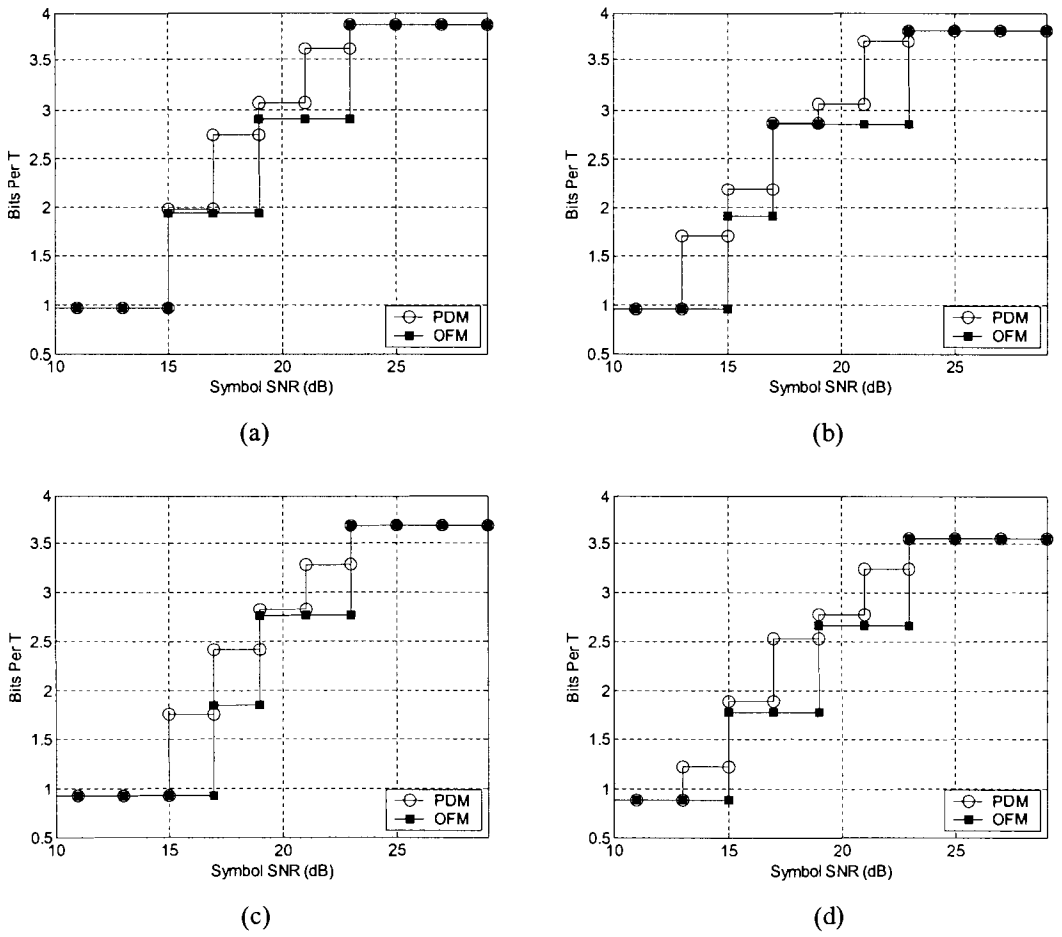

Figure 4-3. Throughput using analog feedback; $L = 4$, $D = 4$, PDM and OFM at $BER_{Tgt} = 10^{-3}$. (a) $f_dT = 0.002$ and $N = 128$, (b) $f_dT = 0.002$ and $N = 84$, (c) $f_dT = 0.005$ and $N = 52$, and (d) $f_dT = 0.005$ and $N = 36$.

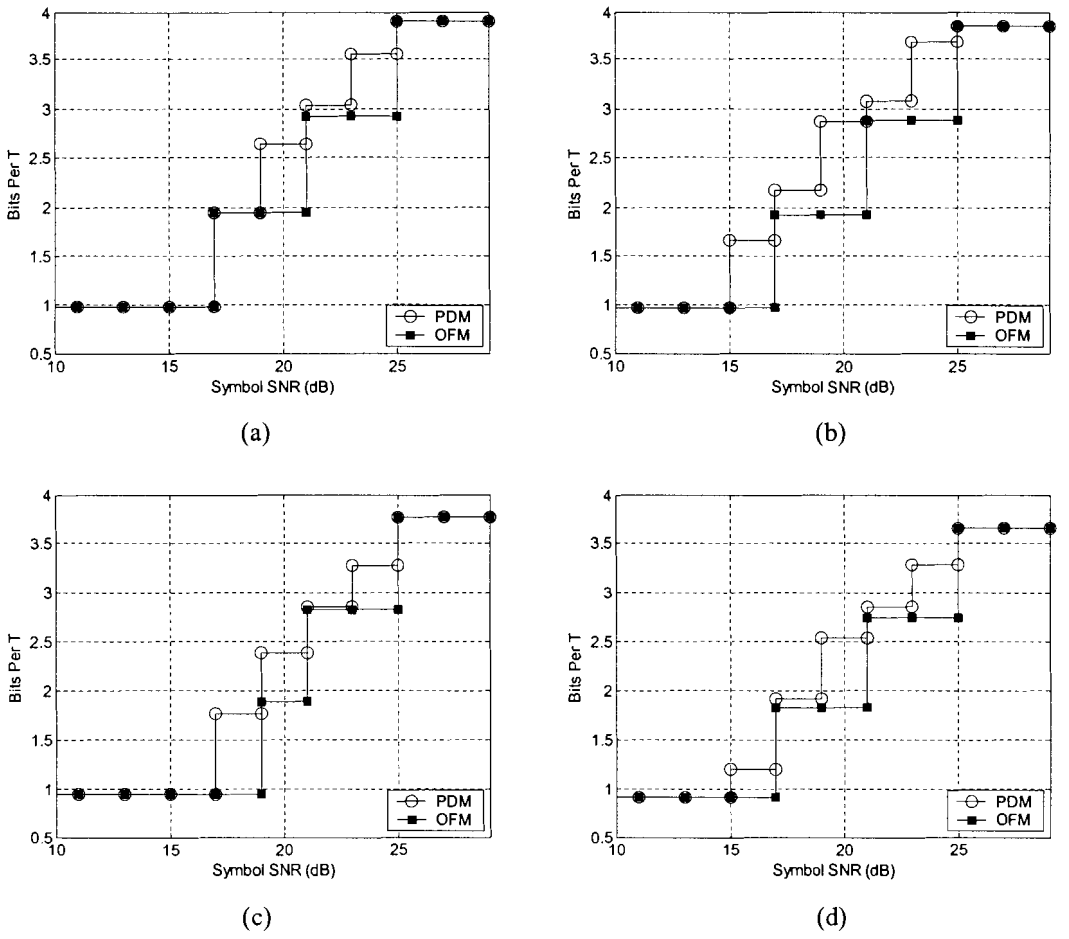

Figure 4-4. Throughput using analog feedback; $L = 3$, $D = 3$, PDM and OFM at $BER_{Tgt} = 10^{-3}$. (a) $f_dT = 0.002$ and $N = 127$, (b) $f_dT = 0.002$ and $N = 83$, (c) $f_dT = 0.005$ and $N = 51$, and (d) $f_dT = 0.005$ and $N = 35$.

4.3 Impacts of Feedback Delay and Frame Size

As evident from the preceding discussion, the proposed closed-loop transmit diversity system, in conjunction with PDM, can yield better performance than traditional systems. In addition, with channel prediction in the proposed system, it is expected to have improved robustness against the impact of feedback delay (see also [7], [9]). The previous simulation results are for short feedback delays (see Table 3-1); here we present simulation results for delays on the order of a few percent of the channel coherence time, i.e.,

$$\frac{\text{Feedback delay}}{\text{Channel coherent time}} = \{2\%, 4\%, 6\%\}.$$

We show in Figure 4-5 and Figure 4-6 the throughput curves of the proposed system, where the simulations are defined by the parameters listed in Table 4-1. As indicated in Section 3.1, to accommodate for longer feedback delays, the downlink channel predictor needs to forecast further into the future (see Figure 3-1 and Figure 3-2), and so the gain estimates are less accurate and beamforming is less effective. Consequently, it is observed that the achievable throughput is reduced gradually with longer feedback delays.

Another issue that we address here is the impact of different frame sizes. As indicated in Section 3.3, BER performance improves with shorter frame sizes – since the range of downlink channel prediction is shortened and ultimately beamforming is more effective – but throughput is likely affected because pilot insertion and feedback rates are higher. However, it can be seen from the results in Figure 4-7 that higher downlink throughput can be achieved with shorter frame sizes at low to mid SNR. For example, in the case in Figure 4-7 (d), we compare the throughput curves for frame sizes of $N = 52$ and $N = 36$, whereby 8% and 11% of the transmission time, respectively, are lost for transmitting a 4-symbol long pilot sequence per downlink frame. Note that below 23 dB SNR the same or higher throughput can be achieved with a shorter frame size because the BER's are lower at every data symbol position, so that at the target BER more symbols can be modulated using larger constellation sizes and carry more bits. But beyond 23 dB SNR, most symbols across the downlink frame are modulated with the largest constellation size, and so a longer frame size can achieve a higher throughput.

Table 4-1. Simulation parameters with different feedback delays.

Base antennas L	Normalized Doppler frequency f_dT	Channel coherence time $1/f_d$	Frame size N	Feedback delay D	Prediction filter order J	PDM target BER BER_{Tgt}
4	0.002	$500T$	128	4, 10, 20, 30	10	10^{-3}
			84			
	0.005	$200T$	52	4, 8, 12		
			36			
3	0.002	$500T$	127	3, 10, 20, 30		
			83			
	0.005	$200T$	51	3, 4, 8, 12		
			35			

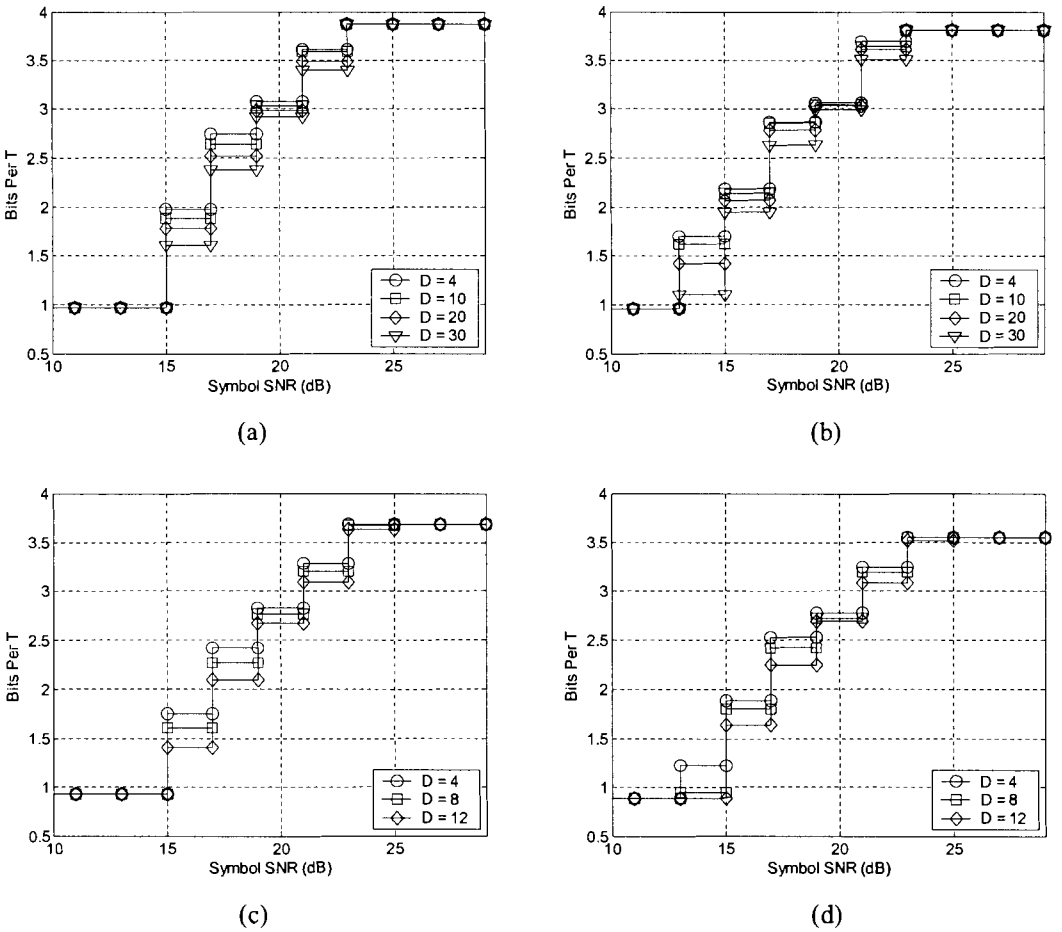

Figure 4-5. Throughput using analog feedback with different delays; $L = 4$ and PDM at $BER_{Tgt} = 10^{-3}$.
(a) $f_dT = 0.002$ and $N = 128$, (b) $f_dT = 0.002$ and $N = 84$, (c) $f_dT = 0.005$ and $N = 52$, and (d) $f_dT = 0.005$ and $N = 36$.

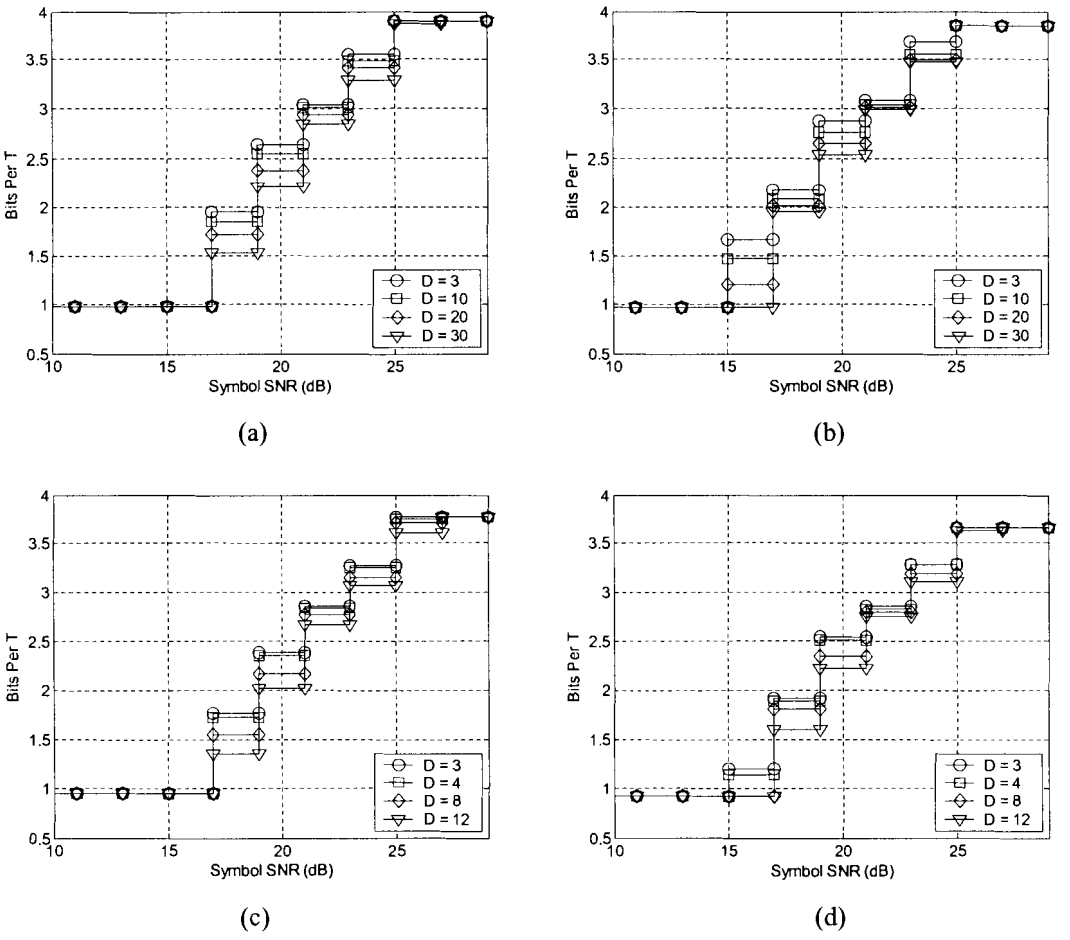

Figure 4-6. Throughput using analog feedback with different delays; $L = 3$ and PDM at $BER_{Tgt} = 10^{-3}$.
(a) $f_dT = 0.002$ and $N = 127$, (b) $f_dT = 0.002$ and $N = 83$, (c) $f_dT = 0.005$ and $N = 51$, and (d) $f_dT = 0.005$ and $N = 35$.

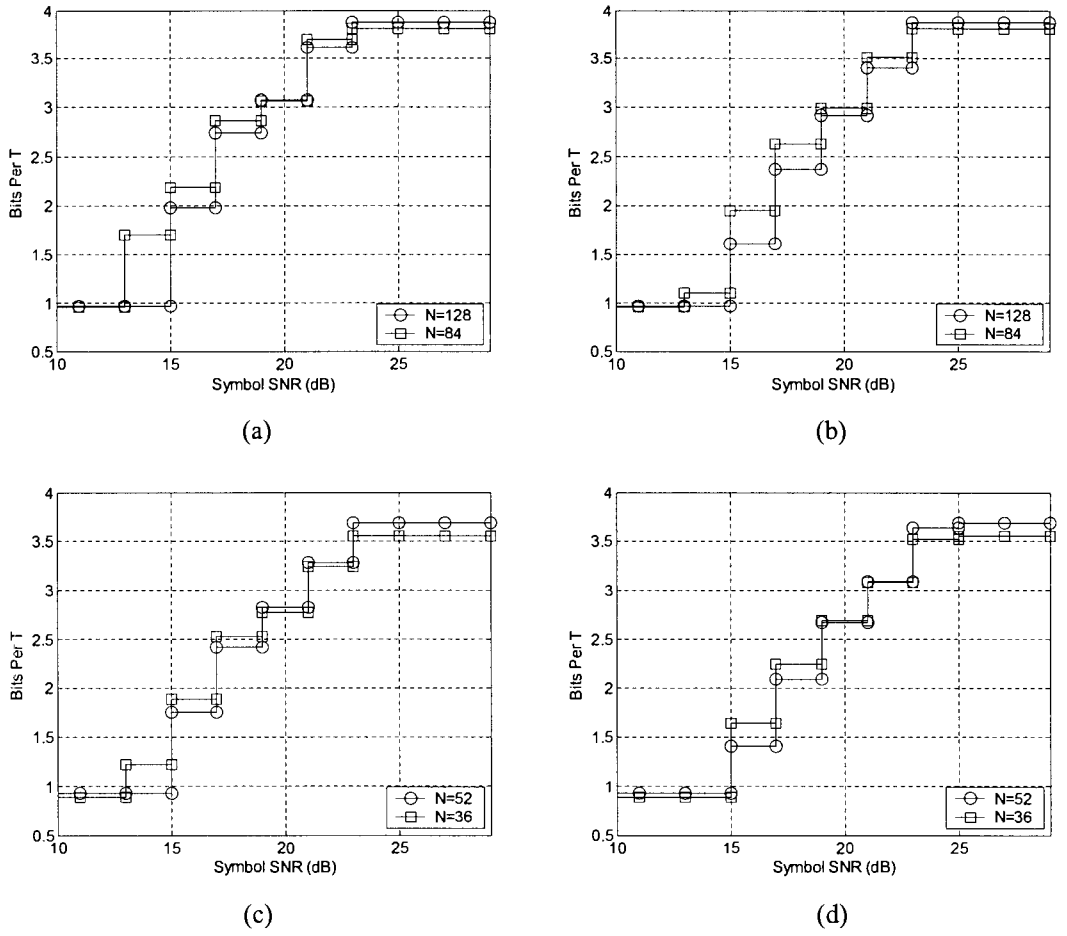

Figure 4-7. Throughput using analog feedback with different frame sizes; $L = 4$ and PDM at $BER_{Tgt} = 10^{-3}$.
(a) $f_dT = 0.002$ and $D = 4$, (b) $f_dT = 0.002$ and $D = 30$, (c) $f_dT = 0.005$ and $D = 4$, and (d) $f_dT = 0.005$ and $D = 12$.

4.4 Limited Peak Power Analog Feedback

The proposed analog feedback scheme has many advantages, but its implementation is technically challenging. As per (30) the analog CSI symbols

$$u_l \equiv u[mN + (l-1) + D] = \frac{\ddot{g}_l[mN + (l-1)]}{\sqrt{2\sigma_{\ddot{g}}^2}},\ l = 1,2,\ldots,L,$$

are samples of Gaussian sources and may thus have high instantaneous power. Therefore, ideal analog feedback requires the mobile transmitter to have a large dynamic

range, which may not be feasible in practice. Nevertheless, this issue can be resolved with a minor compromise. To facilitate analog feedback, we introduce a transmit power clipping threshold P_{Clp} such that

$$u_l = \begin{cases} u_l & |u_l|^2 \le P_{Clp} \\ \sqrt{\frac{P_{Clp}}{|u_l|^2}} u_l & |u_l|^2 > P_{Clp}, \ l = 1,2,\ldots,L. \end{cases} \tag{47}$$

As (47) reveals, clipping retains the phase information embedded in the CSI symbols u_l's, but causes distortion in the amplitude information. Consequently, analog feedback with power clipping will introduce unrecoverable error in the feedback CSI. The performance degradation that results depends on the probability that the symbol power $|u_l|^2$ exceeds the clipping threshold P_{Clp}, and sample values are listed in Table 4-2, where $\Pr\{\cdot\}$ denotes the probability of an event, and P_{Max} represents the peak to mean power ratio of an analog or digital symbol. For instance, analog feedback with $P_{Max} = 6\,\text{dB}$, i.e., P_{Clp} of 4 times the mean power, has a probability of clipping of only 0.02, and so there should be minor performance loss relative to ideal analog feedback. In comparison with the peak to mean power ratios in digital modulations such as 16QAM and 64QAM, we see that it is realistic to implement analog feedback with $P_{Max} = 3\,\text{dB}$, i.e., P_{Clp} of 2 times the mean power. However, given a probability of clipping of 0.14, it should incur some performance loss relative to ideal analog feedback.

Table 4-2. Peak power of analog feedback symbols and probability of clipping.

Analog CSI Symbols				Digital Symbols	
Mean power $\frac{1}{L}\sum_{l=1}^{L} E\left[\lvert u_l \rvert^2\right]$	Clipping threshold P_{Clp}	Probability of clipping $\Pr\left\{\lvert u_l \rvert^2 > P_{Clp}\right\}$	Peak power / mean power P_{Max}	Modulation	Peak power / mean power P_{Max}
1	2	0.14	3 dB	16QAM	2.55 dB
	4	0.02	6 dB	64QAM	3.68 dB

We show in Figure 4-8 to Figure 4-13 the downlink BER and throughput curves using analog feedback with power clipping, where the simulations are defined by the parameters listed in Table 4-1. For reference, we include the performance curves using ideal analog feedback without power clipping and digital feedback with 16QAM symbols.

Consider first the downlink BER curves in Figure 4-8 and Figure 4-9. For simplicity, we only show the results when the base station is equipped with 4 antennas. As expected, analog feedback with $P_{Max} = 6\,\text{dB}$ causes negligible loss in performance when compared to the case of no clipping. On the other hand, it can be seen that analog feedback with $P_{Max} = 3\,\text{dB}$ can still yield comparable performance in the useful BER range of 10^{-4} and above. The SNR loss is at most 1 dB for differential BPSK and 2 dB for differential 8PSK. But unlike ideal analog feedback, since power clipping introduces unrecoverable error in the feedback CSI, the effectiveness of beamforming stops improving at high SNR. Consequently, our use of conventional DD causes the BER curves to show error floors. Note that the use of shorter frame sizes suppresses the error floor, perhaps because a power clipped (and distorted) feedback CSI symbol would be used for the beamforming of fewer data symbols. This, in conjunction with previous

observations, suggests that a suitably chosen data frame size can improve BER performance.

From the downlink throughput curves in Figure 4-10 to Figure 4-13, it can be seen that analog feedback, with and without power clipping, is superior to digital feedback with 16QAM symbols. Note that only minor losses are observed even when the analog feedback symbols have a peak to mean power ratio as low as 3 dB. Therefore, analog feedback, with a suitably chosen transmit power clipping threshold, can in fact be implemented effectively without the need for the mobile transmitter to have a large dynamic range.

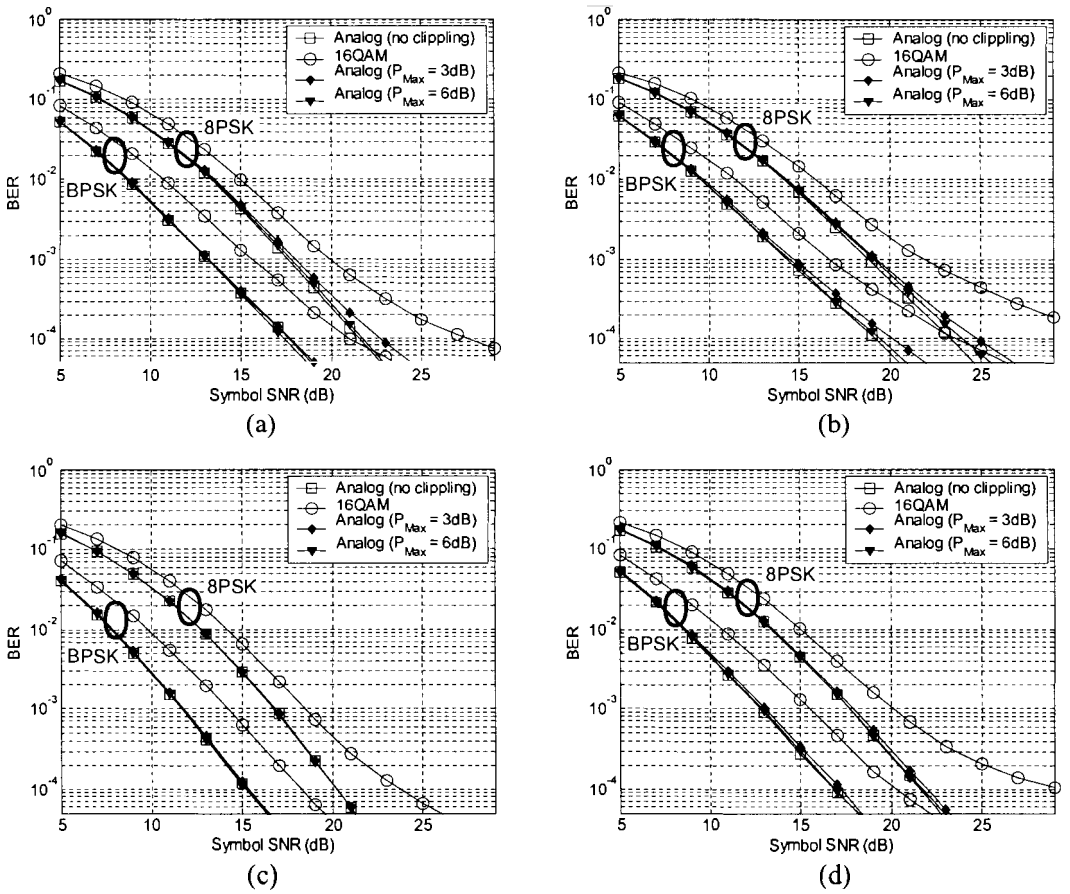

Figure 4-8. Bit error rate of differential BPSK and 8PSK using analog feedback with power clipping; $f_dT = 0.002$ and $L = 4$.
(a) $N = 128$ and $D = 4$, (b) $N = 128$ and $D = 30$, (c) $N = 84$ and $D = 4$, and (d) $N = 84$ and $D = 30$.

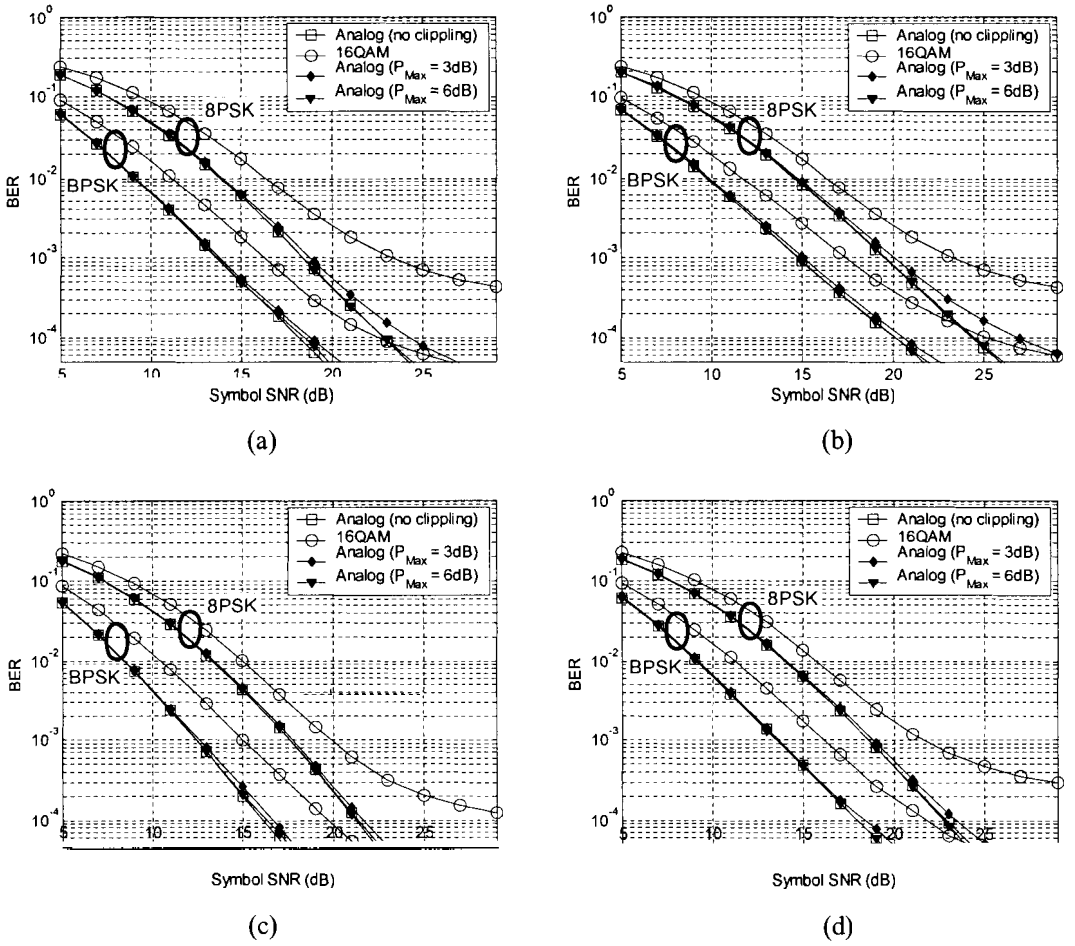

Figure 4-9. **Bit error rate of differential BPSK and 8PSK using analog feedback with power clipping; $f_dT = 0.005$ and $L = 4$.**
(a) $N = 52$ and $D = 4$, (b) $N = 52$ and $D = 12$, (c) $N = 36$ and $D = 4$, and (d) $N = 36$ and $D = 12$.

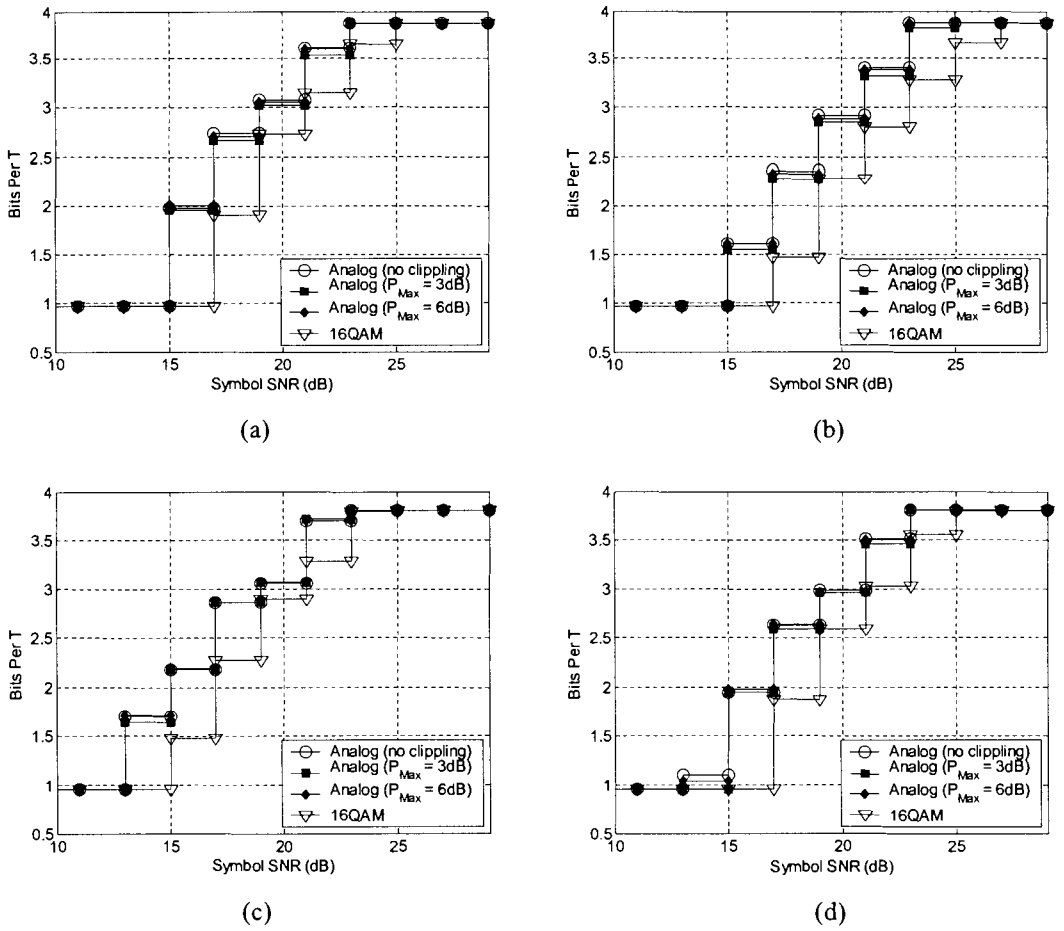

Figure 4-10. Throughput using analog feedback with power clipping; $f_dT = 0.002$, $L = 4$, and PDM at $BER_{Tgt} = 10^{-3}$.
(a) $N = 128$ and $D = 4$, (b) $N = 128$ and $D = 30$, (c) $N = 84$ and $D = 4$, and (d) $N = 84$ and $D = 30$.

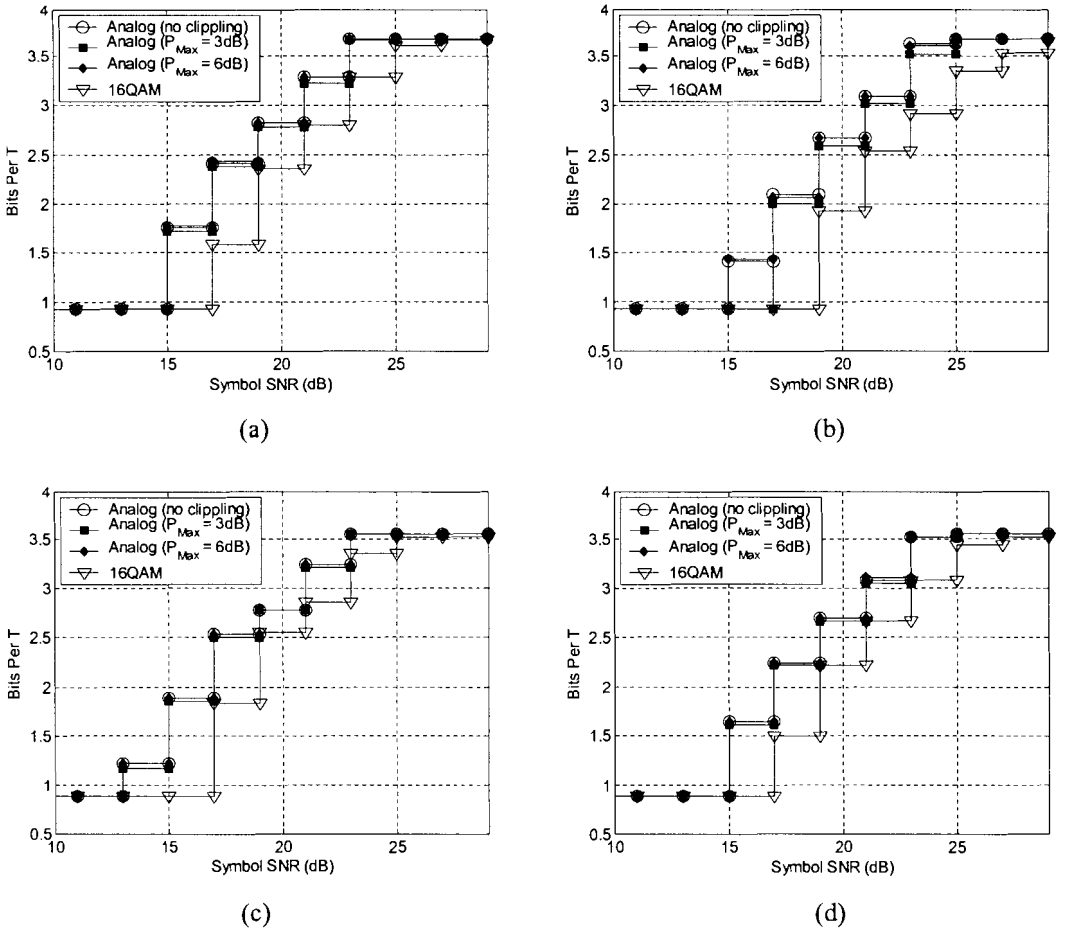

Figure 4-11. Throughput using analog feedback with power clipping; $f_dT = 0.005$, $L = 4$, and PDM at $BER_{Tgt} = 10^{-3}$.
(a) $N = 52$ and $D = 4$, (b) $N = 52$ and $D = 12$, (c) $N = 36$ and $D = 4$, and (d) $N = 36$ and $D = 12$.

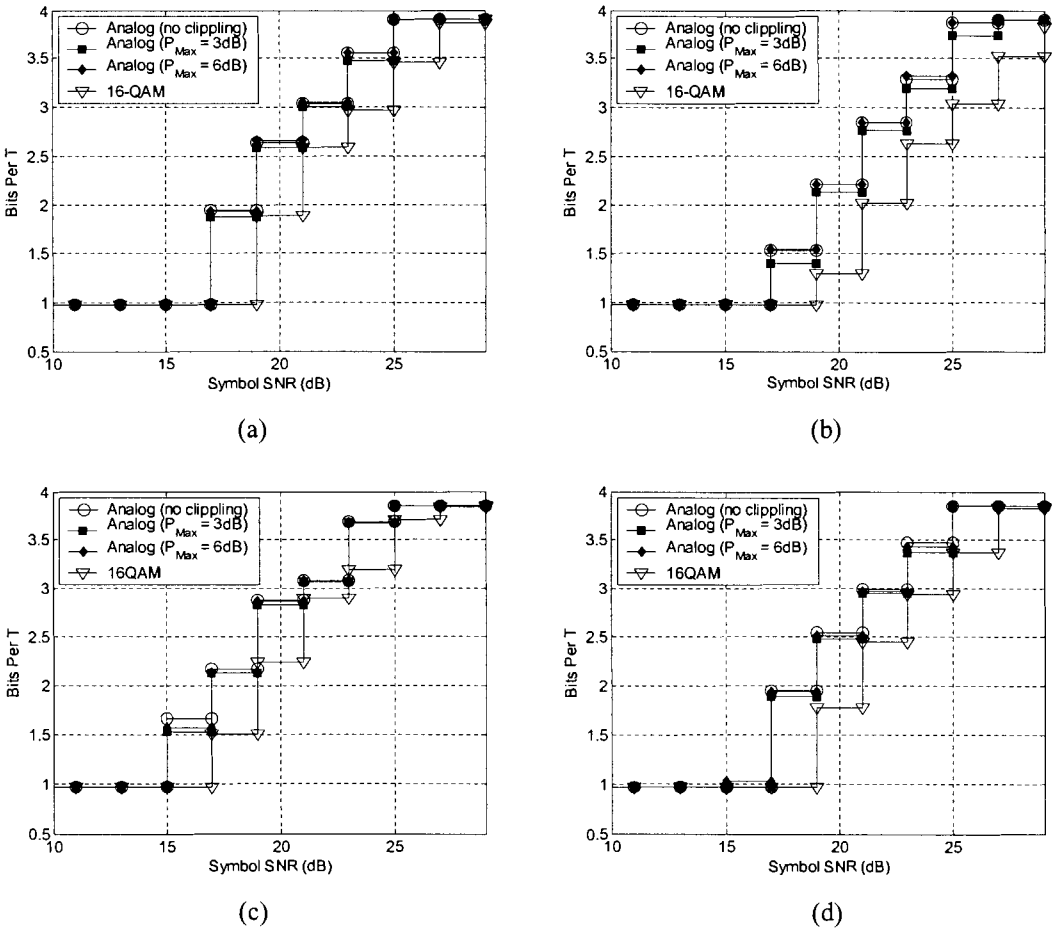

Figure 4-12. Throughput using analog feedback with power clipping; $f_dT = 0.002$, $L = 3$, and PDM at $BER_{Tgt} = 10^{-3}$.
(a) $N = 127$ and $D = 3$, (b) $N = 127$ and $D = 30$, (c) $N = 83$ and $D = 3$, and (d) $N = 83$ and $D = 30$.

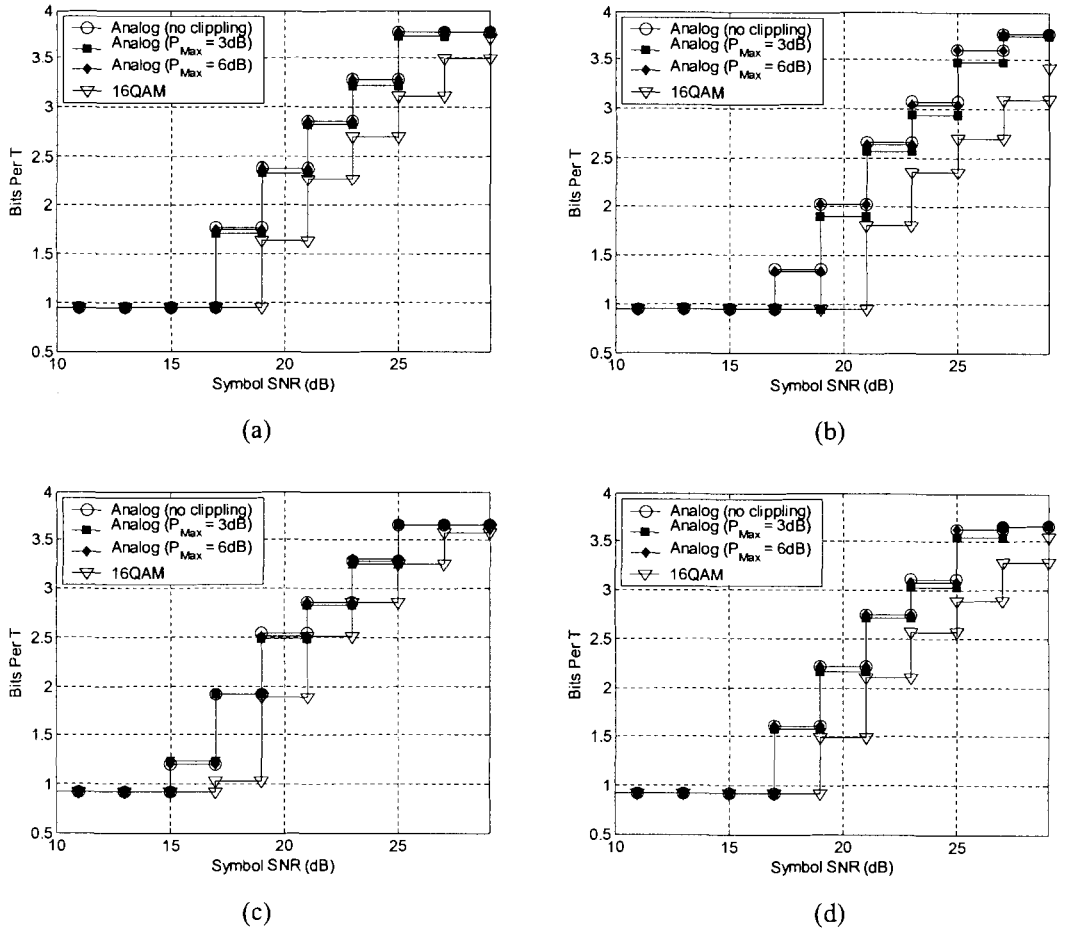

Figure 4-13. Throughput using analog feedback with power clipping; $f_dT = 0.005$, $L = 3$, and PDM at $BER_{Tgt} = 10^{-3}$.
(a) $N = 51$ and $D = 3$, (b) $N = 51$ and $D = 12$, (c) $N = 35$ and $D = 3$, and (d) $N = 35$ and $D = 12$.

4.5 Summary

In this chapter, we identified and provided solutions for various issues associated with the closed-loop transmit diversity system proposed in Chapter 3. First, we considered and ruled out the feasibility of employing MSDD in the downlink as it is found to have little performance advantage over employing conventional DD. Next we dealt with the periodic variation in CSI accuracy using a variable rate position dependent modulation scheme that maximizes the downlink throughput at the given target BER. We investigated how the proposed closed-loop system is affected by feedback delay and

data frame size. It was found that a large feedback delay can significantly reduce the downlink throughput. On the other hand, it was found that a suitably chosen data frame size can improve downlink BER and increase throughput. Finally, we verified that a very small transmit power clipping threshold can be used to limit the dynamic range of the analog feedback symbols, while only incurring minor performance degradation relative to ideal analog feedback.

CHAPTER 5 CONCLUSIONS

In this thesis, we study the downlink performance of a closed-loop transmit diversity system based on analog CSI feedback. We present an analog feedback scheme whereby the mobile unit directly sends back downlink gain estimates to the base station, which in turn applies the knowledge for transmit beamforming. Such an approach is profoundly different from traditional digital feedback schemes whereby the mobile unit sends back quantized downlink gain estimates to the base station.

The use of analog symbols for CSI feedback has two main advantages. First, the scheme requires a low feedback rate of only one symbol per base station antenna per data frame. Second, the scheme does not involve quantization and avoids unrecoverable distortion inherent in digital feedback. The downlink BER and throughput of the proposed system are evaluated via computer simulation. In comparison with results obtained using digital feedback under the same operating conditions, it is observed that analog feedback always yields superior performance.

Various issues associated with the proposed system are identified and addressed, which include the potential gain by employing MSDD in the downlink, the varying beamforming effectiveness across a downlink data frame, the impacts of feedback delay and data frame size, and the large dynamic range of analog feedback symbols. The observations and solutions are summarized below:

a) The use of MSDD has minor performance advantage over conventional DD.

b) To accommodate the periodic variation in beamforming effectiveness, we make use of a variable rate position dependent modulation scheme that can substantially increase the downlink throughput, relative to optimal fixed modulation, at the given target BER.

c) Large feedback delay reduces the timeliness of feedback CSI, and therefore can significantly affect the downlink throughput.

d) A suitably chosen data frame size can improve downlink BER and increase throughput at low SNR.

e) The performance of analog feedback is only slightly affected with a power clipping threshold comparable to the peak power levels in QAM modulations.

Suggestions for Future Research

Possible future extensions to this thesis include further enhancing the proposed analog CSI feedback scheme as well as investigating the performance of analog feedback in other operating environments.

In the proposed analog feedback scheme, downlink gain estimates acquired by the mobile unit are fed back to the base station as is, except for amplitude scaling and power clipping. In this way, however, the interference embedded in the downlink gain estimates is also affected by uplink fading. Instead, we can filter the downlink gain estimates to suppress interference before feeding it back, and this should improve the accuracy of feedback downlink gain estimates.

In this thesis we consider a single-user operating environment, and assume the mobile unit is equipped with a single antenna. Extensions might involve investigating the

performance of analog feedback under a multi-user operating environment, or a single user with multiple antennas. We predict that in both of these applications, analog feedback will also provide superior performance over traditional digital feedback.

The MSE of CSI using analog feedback under a multi-user operating environment is studied in [14]. To complement these results, we can study the downlink BER and throughput as done in this thesis. For instance, we can incorporate analog feedback into the multi-user transmit beamforming framework proposed in [8], which balances between beamforming for each user and interference mitigation. On the other hand, if the mobile unit is equipped with multiple antennas, we can use analog feedback in conjunction techniques such as the two-dimensional beamforming scheme proposed in [25].

APPENDIX A NOISE VARIANCE ON FEEDBACK DOWNLINK GAIN ESTIMATES USING ANALOG FEEDBACK

If uplink channel estimation is accurate, then as per (34) the distortion produced by analog feedback can be modelled as the additive white non-Gaussian noise term $\sqrt{2\sigma_{\ddot{g}}^2}H[mN+(l-1)+D]$ with zero mean and variance

$$\begin{aligned}
&\frac{1}{2}E\left[\left|\sqrt{2\sigma_{\ddot{g}}^2}H[mN+(l-1)+D]\right|^2\right] \\
&= 2\sigma_{\ddot{g}}^2\frac{1}{2}E\left[\left|H[mN+(l-1)+D]\right|^2\right] \\
&= 2\sigma_{\ddot{g}}^2\sigma_v^2E\left[1\Big/\sum_{a=1}^{L}\left|\hat{h}_a[mN+(l-1)+D]\right|^2\right], \\
&= 2\sigma_{\ddot{g}}^2\sigma_v^2E\left[1\Big/\sum_{a=1}^{L}\left|h_a[mN+(l-1)+D]\right|^2\right],
\end{aligned} \tag{48}$$

where the third step follows from (32), and the forth step follows from the assumption of accurate uplink channel estimation, i.e., $\hat{h}_a[mN+(l-1)+D]\approx h_a[mN+(l-1)+D]$. The term $E\left[1\Big/\sum_{a=1}^{L}\left|h_a[mN+(l-1)+D]\right|^2\right]$ averages out the effect of the uplink gains $h_a[mN+(l-1)+D]$'s, which we define below.

Consider first the random variable $\gamma_h=\sum_{a=1}^{L}\left|h_a[mN+(l-1)+D]\right|^2$. Since the uplink gains $h_a[mN+(l-1)+D]$, $a=1,2,\ldots,L$, are independent complex Gaussian random variables, γ_h is χ^2 distributed with a probability density function (pdf) of

$$p_{\gamma_h}(\gamma_h)=\frac{1}{2^L\sigma_h^{2L}(L-1)!}\gamma_h^{L-1}e^{-\frac{1}{2\sigma_h^2}\gamma_h}. \tag{49}$$

It follows that the pdf of the random variable $\Gamma_h=1\Big/\sum_{a=1}^{L}|h_a[mN+(l-1)+D]|^2=1/\gamma_h$ is

$$\begin{aligned} p_{\Gamma_h}(\Gamma_h)&= p_{\gamma_h}\left(\frac{1}{\Gamma_h}\right)\left|\frac{d}{d\Gamma_h}\left(\frac{1}{\Gamma_h}\right)\right| \\ &=\frac{1}{2^L\sigma_h^{2L}(L-1)!}\left(\frac{1}{\Gamma_h}\right)^{L-1}e^{-\frac{1}{2\sigma_h^2}\frac{1}{\Gamma_h}}\frac{1}{\Gamma_h^2}, \end{aligned} \tag{50}$$

and the expected value of Γ_h is defined by

$$\begin{aligned} E[\Gamma_h]&=\int_0^\infty \Gamma_h p_{\Gamma_h}(\Gamma_h)d\Gamma_h \\ &=\int_0^\infty \Gamma_h\left(\frac{1}{2^L\sigma_h^{2L}(L-1)!}\left(\frac{1}{\Gamma_h}\right)^{L-1}e^{-\frac{1}{2\sigma_h^2}\frac{1}{\Gamma_h}}\frac{1}{\Gamma_h^2}\right)d\Gamma_h \\ &=\int_0^\infty \frac{1}{2^L\sigma_h^{2L}(L-1)!}\left(\frac{1}{\Gamma_h}\right)^{L-2}e^{-\frac{1}{2\sigma_h^2}\frac{1}{\Gamma_h}}\frac{1}{\Gamma_h^2}d\Gamma_h. \end{aligned} \tag{51}$$

For mathematical convenience, using the change of variables $\frac{1}{\Gamma_h}=\eta_h$, $-\frac{1}{\Gamma_h^2}d\Gamma_h=d\eta_h$,

(51) becomes

$$\begin{aligned} E[\Gamma_h]&=\int_0^\infty \frac{1}{2^L\sigma_h^{2L}(L-1)!}\left(\frac{1}{\Gamma_h}\right)^{L-2}e^{-\frac{1}{2\sigma_h^2}\frac{1}{\Gamma_h}}\frac{1}{\Gamma_h^2}d\Gamma_h \\ &=\int_\infty^0 \frac{1}{2^L\sigma_h^{2L}(L-1)!}\eta_h^{L-2}e^{-\frac{1}{2\sigma_h^2}\eta_h}(-d\eta_h) \\ &=\frac{1}{2^L\sigma_h^{2L}(L-1)!}\left(-\int_\infty^0 \eta_h^{L-2}e^{-\frac{1}{2\sigma_h^2}\eta_h}d\eta_h\right) \\ &\equiv\frac{1}{2^L\sigma_h^{2L}(L-1)!}\int_0^\infty \eta_h^{L-2}e^{-\frac{1}{2\sigma_h^2}\eta_h}d\eta_h. \end{aligned} \tag{52}$$

Note that the integral $\int_0^\infty \frac{\eta_h^{L-2}}{(L-2)!} e^{-s\eta_h} d\eta_h$, $s = 1/2\sigma_h^2$, represents the Laplace transform of $\eta_h^{L-2}/(L-2)!$ and evaluates to $1/s^{(L-2)+1}$. Taking advantage of this property, (52) can be simplified to

$$\begin{aligned} E[\Gamma_h] &= E\left[1 \Big/ \sum_{a=1}^{L} |h_a[mN + (l-1) + D]|^2 \right] \\ &= \frac{1}{2^L \sigma_h^{2L} (L-1)!} \int_0^\infty \eta_h^{L-2} e^{-\frac{1}{2\sigma_h^2}\eta_h} d\eta_h \\ &= \frac{1}{2^L \sigma_h^{2L} (L-1)!} \left((L-2)! \int_0^\infty \frac{\eta_h^{L-2}}{(L-2)!} e^{-\frac{1}{2\sigma_h^2}\eta_h} d\eta_h \right) \\ &= \frac{1}{2^L \sigma_h^{2L} (L-1)!} \frac{(L-2)!}{\left(\frac{1}{2\sigma_h^2}\right)^{L-1}} \\ &= \frac{1}{(2\sigma_h^2)^L (L-1)(L-2)!} (L-2)! (2\sigma_h^2)^{L-1} \\ &= \frac{1}{2\sigma_h^2 (L-1)}. \end{aligned} \tag{53}$$

Finally, substituting (53) into (48) and $\sigma_{\ddot{g}}^2 = \sigma_g^2 + \sigma_n^2$ as per (28), the noise variance on the feedback downlink gain estimates is thus equal to

$$\begin{aligned} & 2\sigma_{\ddot{g}}^2 \sigma_v^2 E\left[1 \Big/ \sum_{a=1}^{L} |h_a[mN + (l-1) + D]|^2 \right] \\ &= 2(\sigma_g^2 + \sigma_n^2)\sigma_v^2 \frac{1}{2\sigma_h^2 (L-1)} \\ &= \frac{\sigma_g^2 + \sigma_n^2}{L-1} \frac{\sigma_v^2}{\sigma_h^2}. \end{aligned} \tag{54}$$

APPENDIX B QUANTIZER DESIGN FOR DIGITAL FEEDBACK

As indicated in Section 3.2, for digital feedback we encode the I-Q components of each downlink gain estimate $\ddot{g}_l[mN+(l-1)]$ using separate $\sqrt{X}$ -level scalar quantizers. Since the downlink gain estimates $\ddot{g}_l[mN+(l-1)]$'s are circular symmetric and iid, the same quantizer can be used to encode the I-Q components of every channel's gain estimate. Suppose the quantizer maps input values that lies in the partition regions $\widetilde{R}=\{R_1,R_2,\ldots,R_{\sqrt{X}}\}$ into the quantized values $\widetilde{C}=\{C_1,C_2,\ldots,C_{\sqrt{X}}\}$, then a downlink gain estimate $\ddot{g}_l[mN+(l-1)]$ is represented by the quantized value $\widetilde{g}_l[mN+(l-1)]$ according to

$$\begin{aligned}\mathrm{Re}\{\widetilde{g}_l[mN+(l-1)]\}&=\{C_a:\mathrm{Re}\{\ddot{g}_l[mN+(l-1)]\}\in R_a,a=1,2,\ldots,\sqrt{X}\}\\ \mathrm{Im}\{\widetilde{g}_l[mN+(l-1)]\}&=\{C_a:\mathrm{Im}\{\ddot{g}_l[mN+(l-1)]\}\in R_a,a=1,2,\ldots,\sqrt{X}\},l=1,2,\ldots,L.\end{aligned} \tag{55}$$

As per (44) we design the scalar quantizer with the objective to minimize the mean square error distortion

$$\begin{aligned}\varepsilon&=E\left[|\mathrm{Re}\{\widetilde{g}_l[mN+(l-1)]\}-\mathrm{Re}\{\ddot{g}_l[mN+(l-1)]\}|^2\right]\\&=E\left[|\mathrm{Im}\{\widetilde{g}_l[mN+(l-1)]\}-\mathrm{Im}\{\ddot{g}_l[mN+(l-1)]\}|^2\right],\ l=1,2,\ldots,L,\end{aligned}$$

between the downlink gain estimate $\ddot{g}_l[mN+(l-1)]$ and its quantized version $\widetilde{g}_l[mN+(l-1)]$. In the following, we briefly review the quantizer design procedure using the Lloyd algorithm [20 Table 6.1], [21]. For notational convenience, we use $\ddot{g}$ to

denote the I-Q components of the downlink gain estimates. The flow chart of the Lloyd algorithm is shown in Figure B-1. The idea is that, starting with initial choices of partition regions $\widetilde{R}$ and quantized values $\widetilde{C}$, we iteratively refine $\widetilde{R}$ and $\widetilde{C}$ so the quantization distortion ε is reduced until convergence. In particular, at each iteration of the algorithm we adjust the partition regions $\widetilde{R}$ using the nearest neighbor condition whereby the region boundaries are set to the midpoints between two adjacent quantized values

$$R_a = \left\{ \ddot{g} : \frac{C_{a-1} + C_a}{2} < \ddot{g} \le \frac{C_a + C_{a+1}}{2} \right\}, a = 1,2,\ldots,\sqrt{X} \qquad C_0 = -\infty, C_{\sqrt{X}+1} = \infty. \tag{56}$$

It follows that the quantization distortion is given by

$$\varepsilon = \sum_{a=1}^{\sqrt{X}} E\left[\left| C_a - \ddot{g} \right|^2 \middle| \ddot{g} \in R_a \right] \Pr\{\ddot{g} \in R_a\}, \tag{57}$$

where $E[x|y]$ represents the expected value of x given the event y, and $\Pr\{\cdot\}$ denotes the probability of an event. If the quantization distortion ε is not yet converged, then we adjust the quantized values $\widetilde{C}$ to the centroids – the expected values – of the partition regions

$$C_a = E[\ddot{g} | \ddot{g} \in R_a], a = 1,2,\ldots,\sqrt{X}, \tag{58}$$

and proceed to the next iteration of the algorithm. It can be shown that the quantizer obtained as described above is at least locally optimal for the initial choices of partition regions $\widetilde{R}$ and quantized values $\widetilde{C}$.

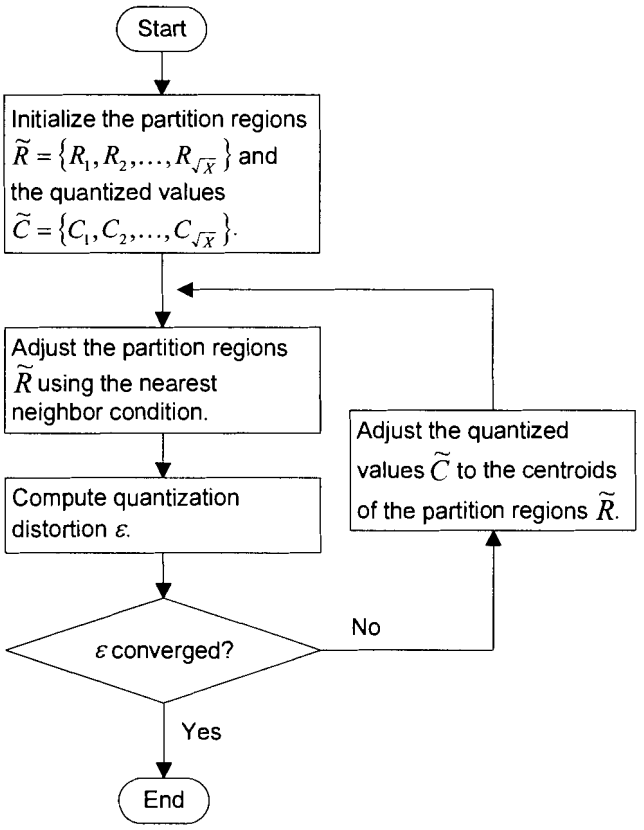

Figure B-1. Flow chart of the Lloyd algorithm.

For the purpose on illustration, we show in Figure B-2 the quantizer designed using the Lloyd algorithm for 4-bit quantization of downlink gain estimates into $X = 2^4 = 16$ levels. The partition region boundaries are shown as dotted lines, and the quantized values are shown as filled circles. Note that the partition regions are rectangular in shape since the I-Q components of downlink gain estimates are encoded using separate scalar quantizers. In addition, the quantized values are more condensed around the mean value of the downlink gain estimates at zero.

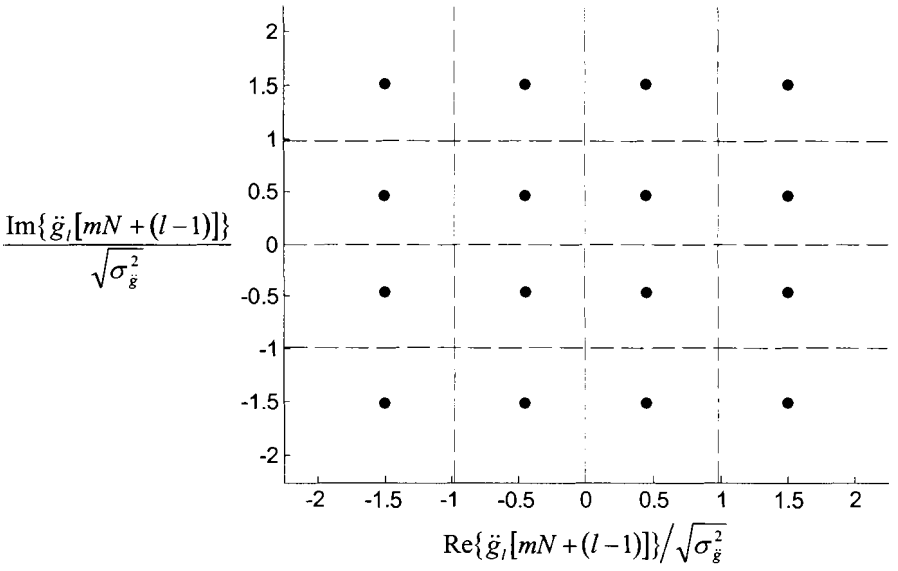

Figure B-2. Quantization of downlink gain estimates into $X = 16$ levels.

REFERENCE LIST

[1] E. Visotsky and U. Madhow, "Space-time transmit precoding with imperfect feedback," *IEEE Trans. Inform. Theory*, vol. 47, pp. 2632-2639, Sept. 2001.

[2] A. Narula, M. J. Lopez, M. D. Trott, and G. W. Wornell, "Efficient use of side information in multiple antenna data transmission over fading channels," *IEEE J. Select. Areas Commun.*, vol. 16, pp. 1423-1436, Oct. 1998.

[3] S. M. Alamouti, "A simple transmit diversity technique for wireless communications," *IEEE J. Select. Areas Commun.*, vol. 16, pp. 1451-1458, Oct. 1998.

[4] V. Tarokh, H. Jafarkhani, and A. R. Calderbank, "Space-time block codes from orthogonal designs," *IEEE Trans. Inform. Theory*, vol. 45, pp. 1456-1467, July 1999.

[5] E. N. Onggosanusi, A. Gatherer, A. G. Dabak, and S. Hosur, "Performance analysis of closed-loop transmit diversity in the presence of feedback delay," *IEEE Trans. Commun.*, vol. 49, pp. 1618-1630, Sept. 2001.

[6] K. C. Hwang and K. B. Lee, "Efficient weight vector representation for closed-loop transmit diversity," *IEEE Trans. Commun.*, vol. 52, pp. 9-16, Jan. 2004.

[7] S. Zhou and G. B. Giannakis, "How accurate channel prediction needs to be for transmit-beamforming with adaptive modulation over Rayleigh MIMO channels?," *IEEE Trans. Wireless Commun.*, vol. 3, pp. 1285-1294, July 2004.

[8] J. K. Cavers, "Single-user and multiuser adaptive maximal ratio transmission for Rayleigh channels," *IEEE Trans. Veh. Technol.*, vol. 49, pp. 2043-2050, Nov. 2000.

[9] S. Hu and A. Duel-Hallen, "Combined adaptive modulation and transmitter diversity using long range prediction for flat fading mobile radio channels," in *Proc. IEEE GLOBECOM'01*, Nov 2001, pp. 1256-1261.

[10] M. Edlund, M. Skoglund, and B. D. Rao, "On the performance of closed-loop transmit diversity with non-ideal feedback," in *Proc. IEEE ICC'03*, May 2003, pp. 3190-3194.

[11] Third Generation Partnership Project (3GPP), "Physical layer procedures," 3GPP TS 25.214 V6.2.0, 2004.

[12] K. K. Mukkavilli, A. Sabharwal, E. Erkip, and B. Aazhang, "On beamforming with finite rate feedback in multiple-antenna systems," *IEEE Trans. Inform. Theory*, vol. 49, pp. 2562-2579, Oct. 2003.

[13] D. J. Love, R. W. Heath, Jr., and T. Strohmer, "Grassmannian beamforming for multiple-input multiple-output wireless systems," *IEEE Trans. Inform. Theory*, vol. 49, pp. 2735-2747, Oct 2003.

[14] T. L. Marzetta and B. M. Hochwald, "Fast transfer of channel state information in wireless systems," submitted to *IEEE Trans. Sig. Proc.*, June 2004. Download available on http://mars.bell-labs.com.

[15] T. J. Goblick, "Theoretical limitations on the transmission of data from analog sources," *IEEE Trans. Inform. Theory*, vol. 11, pp. 558-567, Oct. 1965.

[16] M. Gastpar, B. Rimoldi, and M. Vetterli, "To code, or not to code: lossy source-channel communication revisited," *IEEE Trans. Inform. Theory*, vol. 49, pp. 1147-1158, May 2003.

[17] W. C. Jakes, *Microwave Mobile Communications*. New York: IEEE Press, 1993.

[18] J. K. Cavers, "An analysis of pilot symbol assisted modulation for Rayleigh fading channels," *IEEE Trans. Veh. Technol.*, vol. 40, pp. 686-693, Nov. 1991.

[19] A. Duel-Hallen, S. Hu, and H. Hallen, "Long-range prediction of fading signals," *IEEE Sig. Proc. Mag.*, vol. 17, pp. 62-75, May 2000.

[20] A. Gersho and R. M. Gray, *Vector Quantization and Signal Compression*. Boston: Kluwer, 1992.

[21] Y. Linde, A. Buzo, and R. M. Gray, "An algorithm for vector quantizer design," *IEEE Trans. Commun.*, vol. 28, pp. 84-95, Jan. 1980.

[22] D. Divsalar and M. K. Simon, "Multiple-symbol differential detection of MPSK," *IEEE Trans. Commun.*, vol. 38, pp. 300-308, Mar. 1990.

[23] K. M. Mackenthun, Jr., "A fast algorithm for multiple-symbol differential detection of MPSK," *IEEE Trans. Commun.*, vol. 42, pp. 1471-1474, Feb.-Apr. 1994.

[24] T. H. Cormen, C. E. Leiserson, R. L. Rivest, and C. Stein, *Introduction to Algorithms*, 2nd ed. Cambridge, Massachusetts: MIT Press, 2001.

[25] S. Zhou and G. B. Giannakis, "Optimal transmitter eigen-beamforming and space-time block coding based on channel mean feedback," *IEEE Trans. Sig. Proc.*, vol. 50, pp. 2599-2613, Oct. 2002.

[26] M. K. Simon and M.-S. Alouini, "A unified approach to the performance analysis of digital communications over generalized fading channels," Proc. *IEEE*, vol. 86, pp. 1860-1877, Sept. 1998.

[27] J. G. Proakis, *Digital Communications*, 4th ed. Boston: McGraw-Hill, 2000.

[28] R. F. Pawula, S. O. Rice, and J. H. Roberts, "Distribution of the phase angle between two vectors perturbed by Gaussian noise," *IEEE Trans. Commun.*, vol. 30, pp. 1828-1841, Aug. 1982.